Department of Construction Sciences
Solid Mechanics

ISRN LUTFD2/TFHF-17/5222-SE(1-60)

Topology Optimization for Additive Manufacturing

Master's Dissertation by

Kajsa Söderhjelm

Supervisor:
Mathias Wallin

Examiner:
Ralf Denzer

Printed by Media-Tryck AB, Lund, Sweden
For information, address:
Division of Solid Mechanics, Lund University, Box 118, SE-221 00 Lund, Sweden
Webpage: www.solid.lth.se

Acknowledgement

This master thesis is submitted for a Master's Degree in Mechanical Engineering at the Division of Solid Mechanics, Faculty of Engineering, Lund University.

I would first like to thank my supervisor Professor Mathias Wallin for his guidance and many discussions, this thesis would not exist without his expertise in the field or enthusiasm for research. I would like to thank Niklas Ivarsson for all the help and discussions, especially during our trip to Dalian University of Technology in China. I would also like to thank Professor Jun Yan and Professor Bin Niu at the Dalian University of Technology for their expertise, help, and kind welcoming to China.

Lastly but just as important, I want to thank my dear Björn, my parents and all of my friends for all the love and support.

Lund, November 2017
Kajsa Söderhjelm

Abstract

Topology optimization answers the question "*How to place the material within a prescribed design domain in order to obtain the best structural performance?*" and the design obtained is usually complex. Additive manufacturing comes with a well known design freedom and the design provided by topology optimization can be manufactured without as many constraints as conventional manufacturing methods. However, there does exist a few constraints that needs to be considered such as minimum feature size, enclosed voids, and overhang. This work focus on overcoming the overhang constraint.

A new method proposed by Langelaar (2017) solved with the optimality criteria with a density filter provides printable structures regarding the overhang constraint. The method is very computationally efficient, but the overhang angle is tied to the element discretization and the printing direction needs to be axiparallel to the coordinate axis. This results in that in order to change the inclination angle for the overhang, the element discretization needs to be changed and the printing direction can not be optimized. Instead a new method is proposed using the element density gradients in order alter the design to overcome the overhang constraint. The optimization is solved using the method of moving asymptotes with an extended density based Helmholtz PDE filter. The result shows that the structure is affected by the added constraint. However, the provided design does not provide completely printable structures. Further work is necessary in order to optimize the parameters and get fully printable designs.

Keywords: Topology optimization, additive manufacturing, overhang constraint

Sammanfattning

Topologioptimering svarar på frågan "*Hur placerar man materialet inom en föreskriven designdomän för att uppnå den bästa strukturella prestandan?*" och den erhållna designen blir vanligtvis komplex. Additiv tillverkning kommer med en välkänd designfrihet vilket innebär att designen som tillhandahålls av topologioptimering kan tillverkas utan ett stort antal tillverkningsbegränsningar. Det finns emellertid några bivillkor som måste övervägas såsom minsta detaljstorlek, slutna tomrum och överhäng. Detta arbete fokuserar på att övervinna överhängsbivillkoret.

En ny metod som föreslås av Langelaar (2017) löst med OC-metoden med ett densitetsfilter ger utskrivbara strukturer med avseende på överhängsvillkoret. Metoden är beräkningseffektiv, men överhängsvinkeln är bunden till elementdiskretiseringen och utskriftsriktningen måste vara axiparallell mot koordinataxeln. Detta medför att för att ändra lutningsvinkeln för överhänget behöver elementdiskretiseringen ändras och utskriftsriktningen kan inte optimeras. Istället föreslås en ny metod där densitetsgradienterna för varje element används för att förändra designen och överkomma överhängsbivillkoret. Optimeringen löses med hjälp av MMA-metoden med en variant av Helmholtz PDE filter. Resultatet visar att strukturen har påverkats av filtret, dock är den tillhandahållna designen inte fullständigt utskrivbar. Ytterligare arbete är nödvändigt för att optimera parametrarna och få fullt utskrivbara strukturer.

Nyckelord: Topologioptimering, additiv tillverkning, overhängsbivillkor

Contents

List of Figures

List of Tables

Chapter 1

Introduction

1.1 Background

In the industry, rapid prototyping, RP, is a term that describes a process that rapidly creates a system or a part representation, i.e. creating something fast that will result in a prototype. Additive manufacturing, AM, is a formalized term and was previously denoted rapid prototyping. Additive manufacturing works by creating the part from eg. CAD data adding the material in layers, contrary to the more traditional procedure where material is subtracted. This can be used to shorten the product development times and cost and can be manufactured using both plastic and a variety of metals (Gibson et al., 2015).

Structural optimization focus on making an assemblage of materials sustain loads in the "best" way. The objective could for an example be maximizing the stiffness of a structure. A structural optimization problem consists of an objective function that classifies designs, design variables that describe the design and state variables that represent the response of a structure. There are different types of structural optimization problems and these are sizing optimization, shape optimization and topology optimization. Topology optimization optimizes the material layout in the design space allowing design variables to take the value zero (Christensen et al., 2008). The method is today used in the industry early in the product development to allow designers to investigate structurally efficient concepts. It is integrated in some of the leading FEM softwares today such as ANSYS Mechanical (ANSYS, 2017) and OptiStruct by Altair (OptiStruct, 2017).

The ability of additive manufacturing to manufacture very complex topology, which often is the outcome from topology optimization, makes topology optimization a good design tool for additive manufacturing. In order to ensure manufacturability using additive manufacturing, support material is often necessary to overcome certain constraints such as overhang, minimum feature size, anisotropy to prevent collapsing during fabrication (Clausen, 2016).

This work will target the overhang constraint where the goal is to achieve self-supporting structures without support material. Usually support material is used during manufac-

turing which will increase the print time, the material cost and resources to remove the support structures. Instead of using support structures one could modify the optimal topology to not interfere with the overhang constraint. Leary et al., (2014) proposed a novel method that modifies the optimal topology to enable additive manufacturing. Gaynor and Guest (2016) proposed a method where a combination of local projection to enforce minimum length scale and support region projection address both the minimum feature size constraint and the overhang constraint. Langelaar (2017) presents a method that can be included in conventional density based topology optimization and is implemented with a density filter. The method proposed by Langelaar (2017) comes with many advantages such as time efficiency and the production of self supporting structures. However, in this approach the self-supporting angle is tied to the aspect ratio of the elements and the method requires information about neighbouring elements which for fine meshes or complex domains and geometries become an expensive operation.

The density filter as a solution of Helmholtz PDE by Lazarov and Sigmund (2011) does not require information about the neighbouring elements, thus could become more advantageous to use for finer or more complicated meshes. Another advantageous property with Helmholtz PDE filter is that the method provides nodal values of the filtered design variable. Using the nodal values it becomes simple to calculate the density gradient which in turn could provide an angle between the element gradient and another vector, for example the baseplate vector.

1.2 Aim

The aim of this master thesis is to further examine the method proposed by Langelaar (2017) and to examine the possibility to extend the Helmholtz PDE filter to include the density gradients in the formulation such that a self supporting structure is obtained. Isotropic and linear elastic material will be considered throughout the report and the optimization problem will be solved using the optimality criteria with a density filter for the method proposed by Langelaar (2017). The additive manufacturing filter is provided by Langelaar (2017) and is implemented in MATLAB. The proposed method will be solved using the method of moving asymptotes by Svanberg (1987) with an augmented Helmholtz PDE filter and is implemented in MATLAB and Fortran.

1.3 Structure of Report

The first chapters in the thesis will provide the necessary theory needed for the research. Chapter 2 will derive the finite element formulation. Chapter 3 will provide the necessary information in order to solve the optimization problem. Beginning with the general information regarding structural optimization with focus on topology optimization continuing with solution strategies for the topology optimization problem and filtering techniques. In Chapter 4 the concept of additive manufacturing will be presented. For readers familiar with these subjects it is recommended to move on to Chapter 5. In Chapter 5 state-of-the

art methods regarding constraints for additive manufacturing in topology optimization are presented. In Chapter 6 the method proposed by Langelaar (2017) is examined by presenting the theory regarding the method, testing the method and discussing the result. Chapter 7 proposes a method using an altered Helmholtz PDE filter. The chapter will start by formulating the problem, the topology optimization and filtering. The chapter continues with integrating the overhang constraint into the Helmholtz-type PDE filter and presenting the result. The final chapter, Chapter 8, will discuss the obtained result and further work.

Chapter 2

Finite Element Method

The finite element formulation follows the derivation according to Saabye Ottosen and Ristinmaa (2005). The finite element formulation is based on the weak form which is derived from the equation of balance of linear momentum

$$\int_V \rho \ddot{u}_i dV = \int_V t_i dS + \int_V b_i dv \tag{2.1}$$

where $\rho = \rho(x_i, t)$ is the mass density, $\ddot{u}_i = \ddot{u}(x_i, t)$ is the acceleration field, $t_i = t_i(x_i, t)$ is the traction vector and $b_i = b_i(x_i, t)$ is the body force vector. Using the divergence theorem and that the relation hold for any volume provides the strong form of equation of motion

$$\sigma_{ij,j} + b_i = \rho \ddot{u}_i \tag{2.2}$$

To obtain the weak form equation (2.2) is expressed as

$$\int_V \left[(\sigma_{ij} v_i)_{,j} - \sigma_{ij} v_{i,j} \right] dV + \int_V \left[v_i b_i - \rho v_i \ddot{u}_i \right] dV = 0 \tag{2.3}$$

Using the divergence theorem and the fact that v_i is an arbitrary vector not related to u_i, and defining $\epsilon^v_{ij} = \frac{1}{2}(v_{i,j} + v_{j,i})$ where ϵ^v_{ij} is related to the weight function v_i in the same manner as ϵ_{ij} is related to the displacement u_i as well as symmetry of the stress tensor σ_{ij} provides

$$\int_V \rho v_i \ddot{u}_i dV + \int_V v_{i,j} \sigma_{ij} dV = \int_S v_i t_i dS + \int_V v_i b_i dV \tag{2.4}$$

Exploring the symmetry of σ_{ij} yields

$$v_{i,j} \sigma_{ij} = \epsilon^v_{ij} \sigma_{ij} \tag{2.5}$$

which enables (2.4) to be formulated as the principle of virtual work

$$\int_V \rho v_i \ddot{u}_i dV + \int_V \epsilon^v_{ij} \sigma_{ij} dV = \int_S v_i t_i dS + \int_V v_i b_i dV \tag{2.6}$$

Rewriting this to voigt form provides the following expression

$$\int_V \rho \boldsymbol{v}^T \ddot{\boldsymbol{u}} dV + \int_V (\boldsymbol{\epsilon}^v)^T \boldsymbol{\sigma} dV = \int_S \boldsymbol{v}^T \boldsymbol{t} dS + \int_V \boldsymbol{v}^T \boldsymbol{b} dV \tag{2.7}$$

To be able to express the displacement as an approximation through the entire body using the finite element method, some notations needs to be established. $\boldsymbol{u} = \boldsymbol{u}(x_i, t)$ is the displacement vector, $\boldsymbol{N} = \boldsymbol{N}(x_i)$ is the global shape function, $\boldsymbol{a} = \boldsymbol{a}(t)$ is the nodal displacement, $\boldsymbol{v}$ is the weight function according to the Galerkin method. From this it follows

$$\ddot{\boldsymbol{u}} = \boldsymbol{N}\ddot{\boldsymbol{a}} \qquad \boldsymbol{B} = \boldsymbol{B}(x_i) = \frac{\partial \boldsymbol{N}}{\partial x_i} \qquad \boldsymbol{\epsilon} = \boldsymbol{B}\boldsymbol{a} \qquad \boldsymbol{v} = \boldsymbol{N}\boldsymbol{c} \tag{2.8}$$

The notations in (2.8) put into (2.7) and stating that $\boldsymbol{c}$ is arbitrary provides the notation for the finite element method. Assuming static conditions $\ddot{\boldsymbol{u}} = \boldsymbol{0}$ will result in that the equation of motion is reduced to the equilibrium conditions and becomes

$$\int_V \boldsymbol{B}^T \boldsymbol{\sigma} dV = \int_S \boldsymbol{N}^T \boldsymbol{t} dS + \int_V \boldsymbol{N}^T \boldsymbol{b} dV \tag{2.9}$$

For a linear elastic material the stress tensor can be approximated as $\boldsymbol{\sigma} = \boldsymbol{D}\boldsymbol{\epsilon} = \boldsymbol{D}\boldsymbol{B}\boldsymbol{a}$ where $\boldsymbol{D}$ is the constitutive matrix. For isotropic materials the constitutive matrix $\boldsymbol{D}$ becomes

$$\boldsymbol{D} = \frac{E}{(1+v)(1-2v)} \begin{bmatrix} 1-v & v & v & 0 & 0 & 0 \\ v & 1-v & v & 0 & 0 & 0 \\ v & v & 1-v & 0 & 0 & 0 \\ 0 & 0 & 0 & \frac{1}{2}(1-2v) & 0 & 0 \\ 0 & 0 & 0 & 0 & \frac{1}{2}(1-2v) & 0 \\ 0 & 0 & 0 & 0 & 0 & \frac{1}{2}(1-2v) \end{bmatrix} \tag{2.10}$$

where E is the modulus of elasticity and v is Poisson's ratio. Inserting (2.9) into (2.10) result in

$$\left(\int_V \boldsymbol{B}^T \boldsymbol{D} \boldsymbol{B} dV \right) \boldsymbol{a} = \int_S \boldsymbol{N}^T \boldsymbol{t} dS + \int_V \boldsymbol{N}\boldsymbol{b} dV \tag{2.11}$$

To simplify the method, the stiffness matrix $\boldsymbol{K}$, the load vector $\boldsymbol{f}$ are defined as

$$\boldsymbol{K} = \int_V \boldsymbol{B}^T \boldsymbol{D} \boldsymbol{B} dV \qquad \boldsymbol{f} = \int_S \boldsymbol{N}^T \boldsymbol{t} dS + \int_V \boldsymbol{N}\boldsymbol{b} dV \tag{2.12}$$

Combining (2.11) and (2.12) provide

$$\boldsymbol{K}\boldsymbol{a} = \boldsymbol{f} \tag{2.13}$$

Chapter 3

Optimization

3.1 Structural Optimization

Structural optimization means making a structure sustain loads in the best way. The general mathematical form of a structural optimization problem is usually written as

$$(\$\mathbb{O}) \begin{cases} \text{minimize } g_0(\boldsymbol{x},\boldsymbol{y}) \text{ with respect to } \boldsymbol{x} \text{ and } \boldsymbol{y} \\ \qquad \text{subject to } \begin{cases} \text{behaviorial constraints on } \boldsymbol{y} \\ \text{design constraints on } \boldsymbol{x} \\ \text{equilibrium constraint} \end{cases} \end{cases} \tag{3.1}$$

where g_0 is the objective function which is usually chosen as a minimization problem, i.e. choose g_0 such that a small value is better than a large. The variable that describes the design is the design variable, $\boldsymbol{x}$, which can be changed during the optimization. The last variable, $\boldsymbol{y}$, is called the state variable and represents the response of the structure. There are several types of structural optimization problems: first sizing optimization where the design variable represents a kind of structural thickness, shape optimization where the design variable represents the form or contour of a boundary, and topology optimization. Topology optimization provides an answer to "*How to place the material within a prescribed design domain in order to obtain the best structural performance*?". It was first introduced in a seminal paper by Bendsøe and Kikuchi (1988) where a homogenization method produced an optimal shape as well as topology of a mechanical element. Since its introduction, topology optimization has undergone a huge development in various directions such as density approach, phase field approach and several others.

The formulation in (3.1) is usually referred to as simultaneous formulation since the equilibrium equation is solved simultaneously with the the optimization. If the state variable is uniquely defined for a given design variable, e.g. if $\boldsymbol{K}(\boldsymbol{x})$ is invertible for all $\boldsymbol{x}$ such that $\boldsymbol{u} = \boldsymbol{u}(\boldsymbol{x}) = \boldsymbol{K}(\boldsymbol{x})^{-1}\boldsymbol{F}$, the equilibrium equation can be eliminated from equation (3.1) by treating $\boldsymbol{u}(\boldsymbol{x})$ as a given function and equation (3.1) instead becomes (Christensen et al., 2008)

$$(\mathbb{SO})_{nf} = \begin{cases} \min\limits_{\boldsymbol{x}} g_0(\boldsymbol{x}, \boldsymbol{u}(\boldsymbol{x})) \\ \quad \text{subject to } \left\{ g(\boldsymbol{x}, \boldsymbol{u}(\boldsymbol{x})) \leq 0 \right. \end{cases} \tag{3.2}$$

This formulation is usually called the nested formulation. For large-scale problems the nested formulation becomes more advantageous to use as the number of constraints due to the equilibrium equation becomes large (Christensen et al., 2008). When identifying global minimums of optimization problems the Lagrangian function is used and is defined as

$$\mathcal{L}(\boldsymbol{x}, \boldsymbol{\lambda}) = g_0(\boldsymbol{x}) + \sum_{i=1}^{l} \lambda_i g_i(\boldsymbol{x}) \tag{3.3}$$

where λ_i are called Lagrange multipliers (Christensen et al., 2008). The Karush-Kuhn-Tucker, KKT, conditions are defined below

$$\begin{aligned} \frac{\partial \mathcal{L}(\boldsymbol{x}, \boldsymbol{\lambda})}{\partial x_j} &\leq 0 \qquad \text{if} \qquad x_j = x_j^{max}, \\ \frac{\partial \mathcal{L}(\boldsymbol{x}, \boldsymbol{\lambda})}{\partial x_j} &= 0 \qquad \text{if} \qquad x_j^{min} < x_j < x_j^{max}, \\ \frac{\partial \mathcal{L}(\boldsymbol{x}, \boldsymbol{\lambda})}{\partial x_j} &\geq 0 \qquad \text{if} \qquad x_j = x_j^{min}, \\ \lambda_i g_i(\boldsymbol{x}) = 0, \qquad g_i(\boldsymbol{x}) &\leq 0, \qquad \lambda_i \geq 0, \qquad \boldsymbol{x} \in \chi \end{aligned} \tag{3.4}$$

In order for the KKT points provided by these conditions to be an optimal point the problem needs to be convex. For nonconvex problems there may be KKT points that are not a local optima. For large scale optimization problems the KKT conditions are usually not solved but instead a method called Lagrangian Duality is used (Christensen et al., 2008). Lagrangian Duality maximize the Lagrangian with respect to $\boldsymbol{\lambda} \geq \mathbf{0}$ for a given $\boldsymbol{x}$ which is then minimized with respect to $\boldsymbol{x}$.

$$\min_{\boldsymbol{x} \in \chi} \max_{\boldsymbol{\lambda} \geq 0} \mathcal{L}(\boldsymbol{x}, \boldsymbol{\lambda}) = \min_{\boldsymbol{x} \in \chi} \max_{\boldsymbol{\lambda} \geq 0} \left(g_0(\boldsymbol{x}) + \sum_{i=1}^{l} \lambda_i g_i(\boldsymbol{x}) \right) \tag{3.5}$$

The objective function and constraints are often approximated in such a way that it will be more computationally efficient to solve the so called dual Lagrangian problem which corresponds to (3.5). The dual problem conforming with the primal problem in (3.2) where the the min and max in (3.5) have been interchanged becomes

$$(\mathbb{D}) = \begin{cases} \max\limits_{\boldsymbol{\lambda}} \varphi(\boldsymbol{\lambda}) \\ \quad \text{s.t } \boldsymbol{\lambda} \geq \mathbf{0} \end{cases} \qquad \text{where} \qquad \varphi(\boldsymbol{\lambda}) = \min_{\boldsymbol{x} \in \chi} \mathcal{L}(\boldsymbol{x}, \boldsymbol{\lambda}) \tag{3.6}$$

This generally results in an entirely different function, however if the problem is convex and the following theorem is satisfied the dual problem, equation (3.6), is equal to the primal problem, equation (3.2).

Let the problem be convex and satisfy Slater's constraint qualification (CQ), i.e. there exists a point $\boldsymbol{x} \in \chi$ *such that* $g_i(\boldsymbol{x}) < 0$, $i = 1, ...l$. *Let* x^* *be a local (i.e. also global) minimum of the problem. Then there exists a* $\boldsymbol{\lambda}^*$ *such that* $(\boldsymbol{x}^*, \boldsymbol{\lambda}^*)$ *is a KKT point of the problem.* (Christensen et al., 2008)

The dual objective function, φ, is always concave which means that it is easy to maximize. If $\min_{\boldsymbol{x}\in\chi} \mathcal{L}(\boldsymbol{x}, \boldsymbol{\lambda})$ has one solution for a given $\boldsymbol{\lambda}$ then φ is differentiable at $\boldsymbol{\lambda}$ and can be solved through

$$\frac{\partial \varphi(\boldsymbol{\lambda})}{\partial \lambda_i} = g_i(\boldsymbol{x}^*(\boldsymbol{\lambda})) \qquad i = 1, ..l \quad \text{where} \quad \boldsymbol{x}^*(\boldsymbol{\lambda}) = \min_{\boldsymbol{x}\in\chi} \mathcal{L}(\boldsymbol{x}, \boldsymbol{\lambda}) \tag{3.7}$$

Considering the nested formulation in (3.2), a general topology optimization minimizes an objective function, for instance the compliance, through changing the material distribution as it is subjected to a volume constraint, $G_0 = V \leq 0$ and possibly other constraints $G_i \leq 0, i = 1, .., M$. The design variable, x, could for example describe the thickness of a sheet that has a lower value, ρ_{min} and an upper value ρ_{max} (Christensen et al., 2008). Considering the compliance and discretizing the domain Ω into a large number of finite elements where N describes the element or nodal design variables this becomes

$$\mathbb{SO} = \begin{cases} \min\limits_{\boldsymbol{x}} & C = \boldsymbol{F}^T \boldsymbol{u}(\boldsymbol{x}) \\ s.t. & \begin{cases} \sum v_i x_i - V_{max} \leq 0 \\ G_j(\boldsymbol{u}(\boldsymbol{x}), \boldsymbol{x}) \leq 0, \qquad j = 1, .., M \\ \rho_{min} \leq x_i \leq \rho_{max}, \qquad i = 1, .., N \end{cases} \end{cases} \tag{3.8}$$

3.2 The Method of Moving Asymptotes, MMA

As mentioned before the methods to solve the optimization problems handles convex problems. In reality many problems are non-convex and the solution to solve these problems is to make an convex approximation of it. The method of moving asymptotes, MMA, by Svanberg (1987) provides a strictly convex approximative subproblem which is solved in each step of the iterative process. Other methods similar to the MMA exists, such as convex linearisation or CONLIN, by Fleury and Braibant (1986), where mixed direct or reciprocal design variables are used to get a conservative first order approximation of the objective function. However, the generation of the subproblems in the MMA is controlled by the so called moving asymptotes which both stabilize and speed up the convergence. The method of moving asymptotes is described below and follows the derivation performed in Christensen et al. (2008). The MMA approximation of the function $g_i(x_j)$ where $i = 0, ..., l$ and $j = 1, ..., n$ is

$$g_i^{M,k}(\boldsymbol{x}) = r_i^k + \sum_{j=1}^{n} \left(\frac{p_{ij}^k}{U_j^k - x_j} + \frac{q_{ij}^k}{x_j - L_j^k} \right) \tag{3.9}$$

The L_j and U_j are the moving asymptotes and changes during the iteration procedure but always satisfy $L_j^k < x_j^k < U_j^k$ for the iteration k. r_i^k, p_{ij}^k and q_{ij}^k are defined as

$$p_{ij} = \begin{cases} \left(U_j^k - x_j^k\right)^2 \frac{\partial g_i(\boldsymbol{x}^k)}{\partial x_j} & \text{if} \quad \frac{\partial g_i(\boldsymbol{x}^k)}{\partial x_j} > 0 \\ 0 & \text{otherwise} \end{cases} \tag{3.10}$$

$$q_{ij} = \begin{cases} 0 & \text{if} \quad \frac{\partial g_i(\boldsymbol{x}^k)}{\partial x_j} \geq 0 \\ -\left(x_j^k - L_j^k\right)^2 \frac{\partial g_i(\boldsymbol{x}^k)}{\partial x_j} & \text{otherwise} \end{cases} \tag{3.11}$$

$$r_i^k = g_i(\boldsymbol{x}^k) - \sum_{j=1}^{n} \left(\frac{p_{ij}^k}{U_j^k - x_j} + \frac{q_{ij}^k}{x_j - L_j^k} \right) \tag{3.12}$$

The MMA approximation of the nested formulation in (3.2) becomes

$$\begin{cases} \min\limits_{\boldsymbol{x}} g_0^{M,k}(\boldsymbol{x}) \\ \quad \text{s.t.} \begin{cases} g_i^{M,k}(\boldsymbol{x}) \leq 0, & i = 1, ..., l \\ \alpha_j^k \leq x_j \leq \beta_j^k, & j = 1, ..., n \end{cases} \end{cases} \tag{3.13}$$

where α_j^k and β_j^k are move limits and will be defined below. The MMA approximation is convex and separable which makes the previously discussed Lagrangian Duality a good solution method for solving it. In order to solve the dual Lagrangian problem the derivative of the objective function and the constraint functions with respect to the design variable needs to be solved. This is called the sensitivity analysis and becomes

$$\frac{\partial g_i^{M,k}(\boldsymbol{x}^k)}{\partial x_j} = \frac{p_{ij}^k}{(U_j^k - x_j)^2} - \frac{q_{ij}^k}{(x_j - L_j^k)^2} \tag{3.14}$$

Svanberg (1987) propose the following heuristic approach for updating the asymptotes. For the first two iterations, $k = 0$ and $k = 1$ the asymptotes are updated according to

$$L_j^k = x_j^k - s_{init}(x_j^{max} - x_j^{min}) \tag{3.15}$$

$$U_j^k = x_j^k + s_{init}(x_j^{max} - x_j^{min}) \tag{3.16}$$

where x_j^{min} and x_j^{max} are the lower and upper bound of the design variable and $0 < s_{init} < 1$. In the following iterations the asymptotes depend on the last iteration and the iteration before the last, i.e. $k-1$ and $k-2$. If the $(x_j^k - x_j^{k-1})$ and $(x_j^{k-1} - x_j^{k-2})$ have opposite signs the asymptotes should be forced together in order not to oscillate and are approximated as

$$L_j^k = x_j^k - s_{slower}(x_j^{k-1} - L_j^{k-1}) \tag{3.17}$$

$$U_j^k = x_j^k + s_{slower}(U_j^{k-1} - x_j^{k-1}) \tag{3.18}$$

where $0 < s_{slower} < 1$. However if the sign of $(x_j^k - x_j^{k-1})$ and $(x_j^{k-1} - x_j^{k-2})$ is the same the asymptotes should be further away in order to speed up the convergence and the are approximated as

$$L_j^k = x_j^k - s_{faster}(x_j^{k-1} - L_j^{k-1}) \tag{3.19}$$

$$U_j^k = x_j^k + s_{faster}(U_j^{k-1} - x_j^{k-1}) \tag{3.20}$$

where $s_{faster} > 1$. The design variables should satisfy the constraint in each iteration such that $\alpha_j^k \leq x_j^k \leq \beta_j^k$ where α_j^k and β_j^k are the move limits and are chosen as

$$\alpha_j^k = \max(x_j^{\min}, L_j^k + \mu(x_j^k - L_j^k)) \tag{3.21}$$

$$\beta_j^k = \min(x_j^{\max}, U_j^k + \mu(U_j^k - x_j^k)) \tag{3.22}$$

where $0 < \mu < 1$. This results in that $L_j^k < \alpha_j^k \leq x_j^k \leq \beta_j^k < U_j^k$ which prevent the denominators $U_j^k - x_j^k$ and $x_j^k - L_j^k$ in the approximation equal to zero. In order to make the MMA approximation of the objective function strictly convex usually a term $\varepsilon(U_j^k - x_j^k)/(U_j^k - L_j^k)$ is added to p_{0j}^k and a term $\varepsilon(x_j^k - L_j^k)/(U_j^k - L_j^k)$ is added to q_{0j}^k where $\varepsilon > 0$.

3.3 Solid Isotropic Material with Penalization, SIMP

A commonly used approach to solve topology optimization problems is to introduce some form of penalty to steer the solution to a discrete 0-1 value. This is done by modifying the stiffness matrix for it to depend on a variable that is interpreted as a density of the material. As a result the material distribution is described by the density variable $\rho(\boldsymbol{x})$ that takes either the value 0 for void areas or 1 for solid material. One method that makes use of this is the Solid Isotropic Material with Penalization or SIMP method (Bendsøe and Sigmund, 2004). The SIMP method was originally developed by Zhou and Rozvany (1991) using the approach from Bendsøe (1989) and further investigated by Sigmund and Petersson (1998).

Subsequently, the design variable $\boldsymbol{x}$ will be denoted $\boldsymbol{\rho}$ and the optimization problem minimizing the compliance with a volume constraint becomes

$$\mathbb{SO} = \begin{cases} \min\limits_{\boldsymbol{\rho}} & C = \boldsymbol{F}^T\boldsymbol{u}(\boldsymbol{\rho}) \\ s.t. & \begin{cases} \sum_{i=1}^N v_i\rho_i - V_{max} \leq 0 \\ \rho_{min} \leq \rho_i \leq \rho_{max}, \quad i = 1,..,N \end{cases} \end{cases}$$

Using the SIMP method intermediate designs are penalized by changing the constitutive matrix. For linear elastic material the "effective" Young's modulus takes the form $E(\rho) = \rho^p E$, illustrated in Figure 3.1. A typical value of the constant parameter p is $p = 3$. The optimal solution will provide an almost zero to one solution of the problem. This practically means areas of holes where $\rho = 0$ and regions where Young's modulus is E where $\rho = 1$ (Christensen et al., 2008).

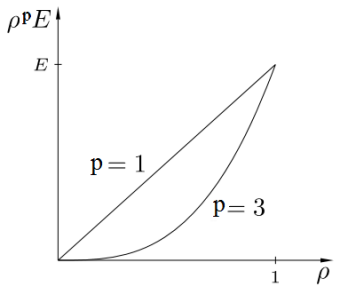

Figure 3.1: The effectiv Young's modulus as a function of ρ^p (Christensen et al., 2008)

In the classical SIMP approach described above the elements with no stiffness is taken into account by the fact that the lower limit, ρ_{min}, imposes a value slightly larger than zero. Instead of this consideration, the modified SIMP approach could be used. Young's modulus instead takes the form

$$E_e(\rho_e) = E_{min} + \rho_e^p(E_0 - E_{min}) \qquad \rho_e \in [0,1] \tag{3.23}$$

The extra variable E_{min} is the stiffness of the void material, still different from zero to avoid singularity of the stiffness matrix. The modified SIMP compared with the classical SIMP comes with a number of benefits, such as covering two-phase design problems and providing a straightforward implementation of additional filters (Sigmund, 2007).

3.3.1 The optimality criteria method, OC, using SIMP

The topology optimization problem could be solved using the MMA approximation but also with the optimality criteria method, or OC method. The OC method is described below and follows the derivation performed in Christensen et al. (2008). The OC method is based on a truncated Taylor approximation of the objective function, here the compliance, which can be expressed as

$$C(\boldsymbol{\rho}) \approx C(\boldsymbol{\rho}^k) + \sum_{e=1}^{n} \left.\frac{\partial C}{\partial y_e}\right|_{\boldsymbol{\rho}=\boldsymbol{\rho}^k} (y_e - y_e^k) \tag{3.24}$$

The intervening variable for the optimality criteria method is $y_e = \rho_e^{-\alpha}$ where $\alpha > 0$. Using this, the derivative of the compliance becomes

$$\frac{\partial C(\boldsymbol{\rho})}{\partial \rho_e} = -(\boldsymbol{u}_e^k)^T \frac{\partial \boldsymbol{K}_M}{\partial \boldsymbol{\rho}} \boldsymbol{u}_e^0 \quad at\ \boldsymbol{\rho} = \boldsymbol{\rho}^k \tag{3.25}$$

where $\boldsymbol{u}(\boldsymbol{\rho}^k) = \boldsymbol{K}_M(\boldsymbol{\rho}^k)^{-1}\boldsymbol{F}$. Using the SIMP approach, the global stiffness matrix is calculated using the effective Young's modulus. Evaluation of $\frac{\partial C}{\partial y_e}$ with (3.24) and (3.25) provides the subproblem:

$$\$\mathbb{O} = \begin{cases} \min\limits_{\boldsymbol{\rho}} \sum\limits_{e=1}^{n} \frac{(\rho_e^k)^{1+\alpha}}{\alpha}((\boldsymbol{u}_e^k)^T p(\rho_e^k)^{p-1} \frac{\partial \boldsymbol{K}_M}{\partial \boldsymbol{\rho}} \boldsymbol{u}_e^k)\rho_e^{-\alpha} \\ s.t \qquad \begin{cases} \boldsymbol{\rho}^T \boldsymbol{a} = V \\ \rho_{min} \le \rho_e \le \rho_{max}, \quad e = 1, ..., n \end{cases} \end{cases} \tag{3.26}$$

Using Lagrangian duality as done before provides the stationary points.

$$\rho_e = \left(\frac{\alpha b_e^k}{\lambda a_e}\right)^{\frac{1}{1+\alpha}} \qquad \text{where} \qquad \rho_e(\lambda) = \begin{cases} \rho_{min} & \text{if} \quad \left(\frac{\alpha b_e^k}{\lambda a_e}\right)^{\frac{1}{1+\alpha}} < \rho_{min} \\ \left(\frac{\alpha b_e^k}{\lambda a_e}\right)^{\frac{1}{1+\alpha}} & \text{if} \quad \rho_{min} \leq \left(\frac{\alpha b_e^k}{\lambda a_e}\right)^{\frac{1}{1+\alpha}} \leq \rho_{max} \\ \rho_{max} & \text{if} \quad \left(\frac{\alpha b_e^k}{\lambda a_e}\right)^{\frac{1}{1+\alpha}} > \rho_{max} \end{cases} \tag{3.27}$$

Inserting this in the Lagrangian function, equation (3.3), to obtain the dual function, equation (3.6), and maximize it to search for it's stationary point provides

$$\frac{\partial \varphi(\lambda)}{\partial \lambda} = \sum_{e=1}^{n} a_e \rho_e(\lambda) - V = 0 \tag{3.28}$$

3.4 Filters

Common numerical problems that appear in topology optimization are checkerboards, mesh dependency and local minimas. Checkerboards refer to regions of alternating solid and void elements ordered in a checkerboard like fashion. Mesh dependence refer to depending on the mesh refinement different optimal solutions are obtained, i.e. the physical explanation is convergence towards microstructure for refinement of the mesh. Local minima refers to that different solutions can be obtained when choosing different algorithmic parameters (Sigmund and Petersson, 1998). In order to avoid these problems filters could be used.

3.4.1 Sensitivity Filter

The sensitivity filter was introduced by Sigmund (1997) and by Sigmund and Petersson (1998). The filter makes the design sensitivity of a given element depend on a weighted average over itself and the eight surrounding neighbour element. The original form of the sensitivity filter is

$$\frac{\partial \tilde{f}}{\partial \rho_e} = \frac{\sum_{i \in N_e} w(\boldsymbol{x}_i)\rho_i}{\frac{\partial f}{\partial \rho_i}\rho_e \sum_{i \in N_e} w(\boldsymbol{x}_i)} \tag{3.29}$$

where the weighting function $w(\boldsymbol{x}_i)$ is a linearly decaying function (Sigmund, 1997). A modification for non-regular meshes where the volume could vary becomes

$$\frac{\partial \tilde{f}}{\partial \rho_e} = \frac{\sum_{i \in N_e} w(\boldsymbol{x}_i)\rho_i \frac{\partial f}{\partial \rho_i}/v_i}{\rho_e / v_e \sum_{i \in N_e} w(\boldsymbol{x}_i)} \tag{3.30}$$

where v_e is the volume of the given element and v_i the volume of each of the surrounding neighbor elements. A major objection is that the sensitivities are modified heuristically and therefore no connection to the objective function exists. However, many applications and physics settings have proven that the sensitivity filtering method converges and is very robust (Sigmund, 2007).

3.4.2 Density Filter

Density filtering was introduced by Bruns and Tortorelli (2001) and mathematically proven as a feasible approach by Bourdin (2001). Density filtering is described below and follows the derivation performed in Sigmund (2007). In density filtering each filtered density is identified as an average of the densities in a neighbourhood of the element. This is performed before doing the finite element analysis and after this is done the sensitivities are modified in a consistent manner. Computing neighbour elements to an element e is performed with a prescribed filter radius R where the spatial center location of element i is $\boldsymbol{x}_i$. The mathematical expression for the neighbourhood surrounding point $\boldsymbol{x}_i$

$$N_e = \{i \mid \|\boldsymbol{x}_i - \boldsymbol{x_e}\| \leq R\} \tag{3.31}$$

The filtered density is calculated by

$$\widetilde{\rho}_i = \frac{\sum\limits_{i \in N_e} w(\boldsymbol{x}_i) v_i \rho_i}{\sum\limits_{i \in N_e} w(\boldsymbol{x}_i) v_i} \tag{3.32}$$

where v_i is the element volume and $w(\boldsymbol{x}_i)$ is a weighting function. The weighting function can be defined in different ways for example as a constant function and by a linearly decaying function, both expressed in (3.33). For a smoother weighting function a Gaussian distribution function can be used.

$$w(\boldsymbol{x}_e) = 1 \qquad\qquad w(\boldsymbol{x}_i) = R - \|\boldsymbol{x}_i - \boldsymbol{x}_e\| \tag{3.33}$$

Using (3.32) and applying the chain rule, the sensitivity of the objective function C with the design variables ρ_e is given by

$$\frac{\partial C}{\partial \rho_e} = \frac{\partial C}{\partial \tilde{\rho}_i} \frac{\partial \tilde{\rho}_i}{\partial \rho_e} \tag{3.34}$$

The adjoint method is used for the sensitivity of the objective function, i.e. the compliance. The first part is derived using the definition of the compliance, $C(\boldsymbol{\rho}) = \boldsymbol{F}^T \boldsymbol{u}(\boldsymbol{\rho})$, where the derivative is

$$\frac{\partial C}{\partial \tilde{\rho}_i} = \boldsymbol{F}^T \frac{\partial \boldsymbol{u}}{\partial \tilde{\rho}_i} = \boldsymbol{u}^T \boldsymbol{K}_M \frac{\partial \boldsymbol{u}}{\partial \tilde{\rho}_i} \tag{3.35}$$

where it is used that $\boldsymbol{K}_M$ is symmetric. In order to obtain $\frac{\partial \boldsymbol{u}}{\partial \tilde{\rho}_i}$ differentiation of the equilibrium equation is performed

$$\frac{\partial \boldsymbol{K}_M}{\partial \tilde{\rho}_i} \boldsymbol{u} + \boldsymbol{K}_M \frac{\partial \boldsymbol{u}}{\partial \tilde{\rho}_i} = \boldsymbol{0} \quad \Longrightarrow \quad \frac{\partial \boldsymbol{u}}{\partial \tilde{\rho}_i} = -\boldsymbol{K}_M^{-1} \frac{\partial \boldsymbol{K}_M}{\partial \tilde{\rho}_i} \boldsymbol{u} \tag{3.36}$$

Inserting (3.36) into (3.35) and the first part in equation (3.34) becomes

$$\frac{\partial C}{\partial \tilde{\rho}_i} = -\boldsymbol{u}^T \frac{\partial \boldsymbol{K}_M}{\partial \tilde{\rho}_i} \boldsymbol{u} \tag{3.37}$$

The second part in equation (3.34) is derived directly from (3.32) and becomes

$$\frac{\partial \tilde{\rho}_i}{\partial \rho_e} = \frac{\sum\limits_{i \in N_e} w(\boldsymbol{x}_i) v_i}{\sum\limits_{i \in N_e} w(\boldsymbol{x}_i) v_i} \tag{3.38}$$

3.4.3 Helmholtz PDE Filter

Popular filtering techniques, for example the mesh independent sensitivity filtering, (Sigmund, 1997) and (Sigmund and Petersson, 1998), and the density filtering, (Bruns and Tortorelli, 2001) and (Bourdin, 2001), requires information about neighbour cells which for fine meshes or complex domains and geometry becomes very computationally expensive to obtain. Lazarov and Sigmund (2011) presented an alternative solution where a Helmholtz-type partial differential equation was used as an alternative to density filtering or sensitivity filtering. The method requires only the mesh information necessary for the finite element discretization of the problem. Density filtering as a solution of Helmholtz PDE is further described below and follows the derivation performed in Lazarov and Sigmund (2011). Helmholtz equation is defined as

$$\nabla^T \boldsymbol{K}_d \nabla \tilde{\rho} + \tilde{\rho} = \rho \qquad \text{where} \qquad \boldsymbol{K}_d = \sum_{i=1}^{d} r_i^2 \boldsymbol{v}_i \boldsymbol{v}_i^T \tag{3.39}$$

The matrix $\boldsymbol{K}_d$ is a positive-definite tensor where the vector $\boldsymbol{v}_i$ is represented as the direction of the length scale r_i, the number of dimensions are defined as d, and the vectors form orthogonal basis $\delta_{i,j} = v_i^T v_i$. If r_i has different values for different i, then anisotropy is introduced. Replacing the vector $\boldsymbol{v}_i$ with the unit vector associated with the coordinate axes and setting $r_i = r_{i+1} = r_{i+d}$ the filter is isotropic. The filtered elemental density is approximated by

$$\tilde{\rho}_e = \boldsymbol{N}_e \tilde{\boldsymbol{\rho}}_e \tag{3.40}$$

The filtered density per element is $\tilde{\rho}_e$ while $\tilde{\boldsymbol{\rho}}_e$ is a vector with the nodal values for element e. $\boldsymbol{N}_e$ consists of finite element interpolation functions. Multiplying the PDE function (3.39) with a weight function, in accordance with Galerkin method: $w = \boldsymbol{N}\boldsymbol{c}$ where $\boldsymbol{c}$ is an arbitrary matrix since w is arbitrary, and integrating over the domain provides the following expression

$$\int_\Omega w \, div(\boldsymbol{K}_d \nabla \tilde{\boldsymbol{\rho}}) d\Omega + \int_\Omega w \, \tilde{\boldsymbol{\rho}} d\Omega = \int_\Omega w \, \rho d\Omega \tag{3.41}$$

Applying Green's formula on equation (3.41), inserting the filtered elemental density equation (3.40) and using that $w = w^T$ result in a system of linear functions for the unknown values of the filtered density.

$$\sum_{i \in N_e} \int_{\Omega_i} [\nabla \boldsymbol{N}_e^T \boldsymbol{K}_d \nabla \boldsymbol{N}_e + \boldsymbol{N}_e^T \boldsymbol{N}_e] d\Omega \tilde{\boldsymbol{\rho}} = \sum_{i \in N_e} \rho_i \int_{\Omega_e} \boldsymbol{N}_e^T d\Omega \tag{3.42}$$

Introducing the matrices $\boldsymbol{K} = \int\limits_{\Omega_i} \nabla \boldsymbol{N}_e^T \boldsymbol{K}_d \nabla \boldsymbol{N}_e d\Omega$, $\boldsymbol{M} = \int\limits_{\Omega_i} \boldsymbol{N}_e^T \boldsymbol{N}_e d\Omega$ and $\boldsymbol{T} = \int\limits_{\Omega_e} \boldsymbol{N}_e^T d\Omega$ allows (3.42) to be reformulated as

$$(\boldsymbol{K} + \boldsymbol{M})\tilde{\boldsymbol{\rho}} = \boldsymbol{T}\boldsymbol{\rho} \tag{3.43}$$

The sensitivity of the objective functions is given by

$$\frac{\partial C}{\partial \rho_e} = \frac{\partial C}{\partial \tilde{\rho}_i}\frac{\partial \tilde{\rho}_i}{\partial \rho_e} \tag{3.44}$$

To evaluate the sensitivity, the adjoint method is used. The second part in (3.44) is given by that $\boldsymbol{K}$, $\boldsymbol{M}$ and $\boldsymbol{T}$ in (3.43) are constant which provides

$$\frac{\partial \tilde{\rho}_i}{\partial \rho_e} = (\boldsymbol{K} + \boldsymbol{M})^{-1}\boldsymbol{T} \tag{3.45}$$

The first part in (3.44) is derived as before in section 3.4.2 and becomes

$$\frac{\partial C}{\partial \tilde{\rho}_i} = -\boldsymbol{u}^T \frac{\partial \boldsymbol{K}_M}{\partial \tilde{\rho}_i}\boldsymbol{u} \tag{3.46}$$

3.5 Thresholding

Filters such as the proposed density filter and Helmholtz PDE filter create smooth transitions between material and void regions, thus densities in the interval $0 \leq \rho \leq 1$ are allowed. To seek a distinct 0/1 solution a thresholding projection filter could be applied on the filtered densities. The filter introduces a length scale into the optimization in order to avoid convergence towards microstructures for fine meshes. The thresholding projection shrinks the length scale and introduces a minimal length scale. Guest et al. (2004) uses a regularized Heaviside step function to achieve this. The thresholding function is approximated as a smooth function governed by a parameter β and the function proposed by Guest et al. (2004) is defined as

$$\bar{\rho}_e = 1 - e^{-\beta\tilde{\rho}_e} + \tilde{\rho}_e e^{-\beta} \tag{3.47}$$

If the parameter $\beta = 0$ results in $\bar{\rho}_e = \tilde{\rho}_e$, however if β approaches infinity the function is approaching a max-operator. Instead of a max-operating function a min operating function can be used. One function proposed by Sigmund (2007) still governed by the parameter β is defined as

$$\bar{\rho}_e = e^{-\beta(1-\tilde{\rho}_e)} - (1 - \tilde{\rho}_e)e^{-\beta} \tag{3.48}$$

The main difference between the two methods is that in the min-operating method material is removed and the opposite is done in the max-operating method where material is added (Sigmund, 2007). Neither of the functions mentioned above is volume preserving which could affect the convergence towards the optimal solution. By combining the max-operating scheme and the min-operating scheme a volume preserving projection method can be obtained and this was proposed by Xu et al. (2010). The function is still governed by the parameter β but now also a new parameter η. The function is defined as

$$\bar{\rho}_e = \begin{cases} \eta\left[e^{-\beta(1-\tilde{\rho}/\eta)} - (1 - \tilde{\rho}/\eta)e^{-\beta}\right] \\ (1-\eta)\left[1 - e^{-\beta(\tilde{\rho}-\eta)/(1-\eta)} + (\tilde{\rho} - \eta)e^{-\beta}/(1-\eta)\right] + \eta \end{cases} \tag{3.49}$$

The three different step functions are illustrated in Figure 3.2 where the parameter β that controls the slope of the function is set to 5 and the parameter η in the volume preserving function moves the center of the graph and is set to 0.5 .

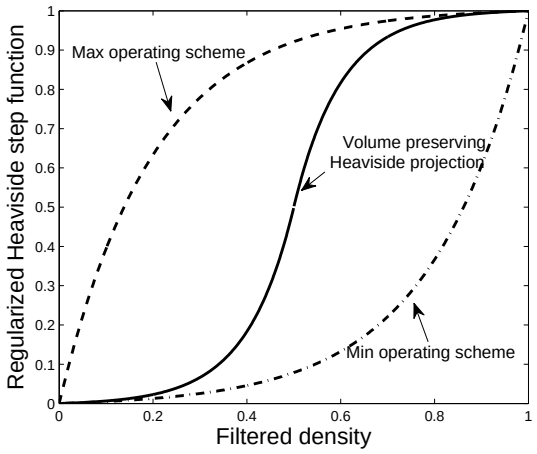

Figure 3.2: Regularized Heaviside step functions.

Chapter 4

Additive Manufacturing

4.1 Rapid Prototyping to Additive Manufacturing

In the industry, rapid prototyping, RP, is a term that describes a process that rapidly creates a system or a part representation, i.e. creating something fast that will result in a prototype. As of today many parts manufactured using the rapid prototyping techniques are directly created and used and we should no longer label these as prototypes. Instead the term additive manufacturing, referred to in short as AM, is used. Additive manufacturing works by creating the parts from three-dimensional Computer-Aided Design, 3D CAD, adding the material in layers, contrary to the more traditional way where material is subtracted instead such as turning or milling. Each layer is a thin cross-section of the part from the original CAD data and the thinner the layer is the closer the result will be to the original. This can be used to shorten the product development times and cost and can be made from both plastic and a variety of metals (Gibson et al., 2015).

4.2 Additive Manufacturing Technologies

The first method to create an object from CAD data was developed in the 1980s. As mentioned before it was mainly used to create prototypes, but as the technology has advanced it is now used to create small series of products. The evolution of additive manufacturing technologies leads to new solutions and methods which also broadens the application areas (Gibson et al., 2015). The additive manufacturing technologies can be divided into laser technologies, flash technologies, extrusion technologies, jet technologies, and lamination and cutting technologies (Gardan, 2016).

The laser technologies include Stereolithography (SLA), Selective Laser Melting (SLM), Selective Laser Sintering (SLS), and Direct Metal Laser sintering (DMLS). In SLA the models are defined by scanning a laser beam over a photopolymer surface. In SLM a thin layer of powder material is applied and a laser beam is projected on lines or points which fuses the powder together by melting the metal. SLS and DMLS works in a similar way as SLM but the sintering process does not fully melt the powder, instead the particles fuses together. In DMLS a laser selectively melts or sinter a thin layer of powder fusing them

together and once the powder is fused the platform moves down and the powder bed is recoated and the process is repeated. A method similar to SLM is Electron-beam melting (EBM) as it also uses powder that melts layer-by-layer. EBM generally has superior build rate compared to SLM due to higher energy density and scanning rate (Gardan, 2016).

The flash technology is derived from the SLA technology in order to reduce lead time and increase build speed. The laser is projected on the entire layer which increases the building speed. Extrusion technologies include Fused Deposition Modelling (FDM), Directed Energy Deposition (DED), and Dough Deposition Modelling (DDM). FDM uses thermoplastic filament extruded from a nozzle to print one cross section of an object. DED is a more complex method usually used to repair or add additional material to existing surfaces and covers laser engineered net shaping, directed light fabrication, direct metal deposition and 3D laser cladding. DDM groups the processes which file different doughs, for instance are a few technologies based on the FDM method but uses a syringe to deposit a dough material. Jet technologies include methods such as Multi Jet Modelling (MJM) and Three-Dimensional printing (3DP) also known as Colour Jet Printing (CJP). MJM uses two different photopolymers when building the part; one is used for the actual model and another for supporting. The supporting material is later removed. Similarly with MJM the 3DP uses powder, for instance metal, that are glued together. The part is later solidified by for example sintering where the glue is removed. Lamination and cutting technologies such as Laminated Object Manufacturing (LOM) is a process where the part is built from layers of paper and uses thermal adhesive bonding and laser patterning (Gardan, 2016).

4.3 Material and Process

A large variety of materials can be used in the different additive manufacturing technologies. Commercial additive manufacturing machines including sheet lamination can process polymers, metals, ceramic materials, paper, wood, cork, foam and rubber. Examples of different materials that can be used can be observed in Figure 4.1 (Clausen, 2016).

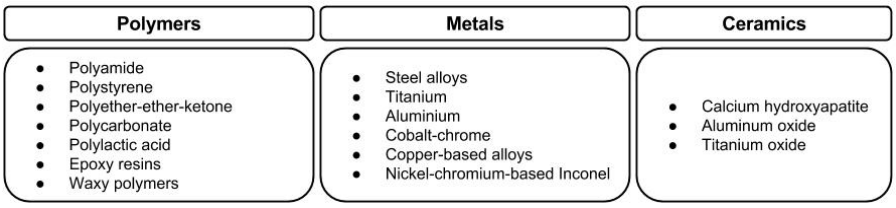

Figure 4.1: Commonly used materials in additive manufacturing.

Gibson et al. (2015) have divided the general process chain for additive manufacturing into eight steps. The process scheme can be observed in Figure 4.2. The first step is to obtain 3D CAD for instance through using a 3D CAD software. The next step will be to convert the 3D CAD data to a STL file format, which nearly every additive manufactur-

ing technology uses. The STL format works by approximating the surfaces of the model with a series of triangular facets. As no units, colors, material or other features are saved as information in a STL file the "AMF" file format is now the international ASTM/ISO standard. The parameters mentioned above is extended to the STL file to be included in the AMF file. Step 3, step 4 and step 5 includes transferring the additive manufacturing ready file to the machine and setting up the machine software parameters and building the component. Step 6 includes removal and cleanup, where the part is removed from the build platform and sometimes also removal of support structure is necessary. Ideally the output from the additive manufacturing machine would be ready for use, but this is unfortunately usually not the case. In step 7 post-processing is the final stage of finishing the part, some of the processes involve chemical or thermal treatment or abrasive finishing such as polishing or application of coatings.

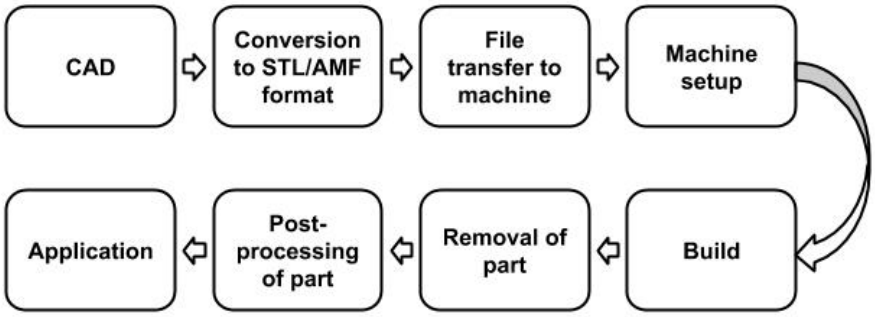

Figure 4.2: The process scheme for additive manufacturing.

There is a wide application for additive manufacturing and the number of applications increase as the process improves. Historically the largest industrial sectors using the additive manufacturing technique are the automotive, health care, consumer products and aerospace sectors. The main reason for the usage in these sectors is the ability to generate complex geometries with a limited number of processing steps. This capability provides an opportunity to physically implement topologically optimal geometries, which are often highly complex (Gibson et al., 2015).

4.4 Manufacturing Constraint

The main advantage of additive manufacturing is its ability to create very complex geometries which would not be possible with conventional methods such as casting. Additive manufacturing provides an opportunity with design freedom. Unfortunately, additive manufacturing comes with manufacturing constraints. These include the digital and physical discretization of the parts to be produced, material capability, overhang, processing time, heat dissipation, the machine and material cost, enclosed voids, layer induced anisotropy, and minimum feature size (Thompson et al., 2016).

Both polymer based processes and powdered metal based processes require support material in order to ensure manufacturability for certain topologies. For example the FDM method, the DMLS method and the SLM method require support structures in order to be able to manufacture certain topologies. In the FDM method support structures surround the the part. It prevents the structural material from distorting for instance through curling because of residual stresses or sagging due to unsupported regions. The support material is removed in a post-print chemical bath. The usage of support structures increase the material usage, print time and require a chemical bath for removal (Vanek et al., 2014). Vanek et al. (2014) defines the critical angle for the FDM process where support structures are needed to 45°, i.e. the printing faces may deviate up to 45° from the printing direction vector in order to be printable without support structures. It is however pointed out that the exact value of the critical angle varies from printer to printer and is not generally accessible.

Metal additive manufacturing, MAM, usually requires support structures to hold the part during the process. The thermal gradient from the selective heating and solidification processes creates residual stresses that leads to significant distortions such as curing and warping in the part (Thomas, 2010). It has been shown that overhanging surfaces warp easier when the inclined angle is smaller. Other parameters such as scanning speed and laser power also affect warping (Wang et al., 2013). The affect of the need of support structures for MAM is similar to when using polymers, it increases the material usage, the print time and the post-fabrication time. The support structures connect the build platform to the part which provides structural resistance against distortion and help with the heat dissipation. By preventing overhang features in the design one might be able to be avoided support stuctures (Thomas, 2010). Thomas (2010) identifies the typical critical angle as to 45° in the DMLS process and Wang et al. (2013) identifies the critical angle to 45° in the SLM process.

Chapter 5

Topology Optimization for Additive Manufacturing

Topology optimization results in an optimal material distribution that is independent of a priori assumption of domain connectivity, and therefore provides an opportunity for innovative structural design. The design obtained from topology optimization is usually very complex. Traditional manufacturing techniques are expensive, and will in some cases even fail, with higher demands on the complexity of the structure. However, when using additive manufacturing this is not the case. Due to the many manufacturing constraints using conventional manufacturing processes the optimized topology requires simplification or constraining of the design space. Combining topology optimization with the design freedom that comes with additive manufacturing could create the perfect couple. Even though the number of constraints in additive manufacturing is not as many as with conventional manufacturing methods they still need to be taken into account. Clausen (2016) divides the constraints into two categories for additive manufacturing oriented topology optimization. The first one is the non-directional constraints which include enclosed voids and minimum feature size. The second category are the directional constraints, characterized by being related to the print direction. Examples of the directional constraints are the layer induced anisotropy, thermal warping and overhang support. There are a few methods where the topology optimization algorithm is combined with constraints regarding additive manufacturing.

5.1 Non-directional constraints

Enclosed voids is a constraint for certain additive manufacturing technologies, eg. SLM and SLS, where powder gets trapped inside the void or FDM. In the FDM method support structures are usually necessary inside a part which are needed to be removed after manufacturing. Various approaches have been suggested to implement this constraint in topology optimization. Shutian et al. (2015) suggested an approach named virtual temperature method (VTM). The voids in the structure are filled with a virtual heating material with high heat conductivity and solid areas are filled with a virtual material with low heat conductivity. The constraint is integrated as a maximum temperature constraint

and can be used as a constraint in topology optimization. Quhao et al. (2016) continues on this approach proposing the generalized method, virtual scalar field method (VSFM) where the temperature field could be one of the scalar fields.

The minimum feature size constraint in additive manufacturing could be compared with the minimum member thickness constraint investigated by Guest et al. (2004) and Poulsen (2003). Poulsen (2003) presents a scheme to implement a minimum length scale in topology optimization. It depends on testing for monotonicity of the restriction of the density function to test lines and is formulated as one constraint. Guest et al. (2004) uses nodal design variables projected by functions based on the minimum length scale onto element space determining the element volume fraction. A more recent publication by Zhou et al. (2015) have presented an approach to achieve minimum length scale based on geometric constraints in a filtering-threshold topology optimization scheme. The approach is based on a density filter combined with a projection scheme. This sort of constraint is also found in commercial softwares such as in OptiStruct by Altair (OptiStruct, 2017).

5.2 Directional constraints

The so called directional constraints defined by Clausen (2016) cause a bit more inconvenience because the print direction plays a huge roll. According to Clausen (2016) the print direction should also be optimized. All the directional constraints such as layer induced anisotropy, thermal warping and overhang should be included to optimize the orientation in which the part should be printed. Thermally induced residual stresses, or thermal warping, come from local melting and nonuniform cooling of the part. The need for support structures in metal printing is mainly due to thermal induced residual stresses and heat dissipation. Li et al. (2016) developed two multiscale modeling methods to be able to predict residual stresses in the parts. The proposed methods are however not validated in reality. The result of layer induced anisotropy is that for certain additive manufacturing methods the print direction will be weaker than the in-plane direction. This could be included in topology optimization using an orthotropic material with one weaker direction and one stiffer direction which is not a problem if the print direction is predefined (Clausen, 2016).

There are a few methods including a constraint to achieve self-supporting structures without support structures. Brackett et al. (2011) provided an overview of the issues and opportunities for application of topology optimization for additive manufacturing. It was proposed that an overhang detection procedure was to be integrated in the topology optimization but no result was reported. Leary et al. (2014) presented a novel method that modifies the theoretically optimal topology to enable additive manufacturing. The method focus on the FDM method which has a problem with overhang. The inclination angle between the plate and the surface was divided into three zones; robust zone ($40^\circ \leq \theta$), compromised zone ($30^\circ \leq \theta < 40^\circ$) and failed zone ($\theta < 30^\circ$). The reported result ensured manufacturability without support material.

Gaynor and Guest (2016) embedded a minimum allowable self-supporting angle extending the filtering procedure, through a series of projection operations, making the part self supporting. A combination of local projection to enforce minimum length scale and support region projection address both the minimum feature size constraint and the overhang constraint. The filter mimics the actual additive manufacturing process as it is applied in a layer-wise manner which according to Gaynor and Guest (2016) is one of two primary disadvantages. This generally result in computational inefficiency since efficient parallel processing can not be utilized with this approach. The method is based on the regularized Heaviside projection method by Guest et al. (2004). It uses two neighbourhood sets, one with the local neighbourhood within a distance, r_{min}, of the element centroid and one set related to the overhang conditions defined as the region that must contain some material for the point to be considered supported. The latter set is limited to those points within a distance, r_s, below the design variable i creating a wedge-shaped region. The filtered density variables are a function of embedded non-linear functions which lead to the second primary disadvantage with the method according to Gaynor and Guest (2016). Thus it leads to convergence issues for more difficult design problems. The published result show that the generated designs are self supporting. However, in need of an additional projection step to remove intermediate densities.

Langelaar (2017) presents a method that can be included in conventional density-based topology optimization. All the elements in the mesh is associated with a blueprint density and gets printed if they are sufficiently supported. Langelaar (2017) targets the SLM and EBM additive manufacturing process where, as mentioned before, the critical angle is $\alpha_c = 45°$. The supported region for a element for the two dimensional case is the three elements below it. This result in that if the angle is set to 45° it has to be square elements. The filter works in a way such that the printed density can't be larger than the maximum density in the supporting region. This results in elements that are not sufficiently supported do not get printed. The reported result show that the models become self supporting but some regions contain intermediate densities and an additional projection step is necessary to get rid of these regions. The additive manufacturing filter has also been extended to the three dimensional case by Langelaar (2016). It works in a similar way as for the two dimensional case, however, the support region now contain the nine elements below. The method presented in Langelaar (2017) for the two dimensional case will be further evaluated in Chapter 6.

Chapter 6

Evaluation of Existing Method

Langelaar (2017) presents a method that can very easily be integrated in a density-based topology optimization algorithm. The method takes the overhang constraint into account, especially targeting SLM and EBM additive manufacturing processes, and the filter mimics the additive manufacturing process by being applied in a layer-by-layer manner.

6.1 Method and Derivation

All the elements in the mesh is associated with a blueprint density variable, $\rho_{(i,j)}$, where the printed density, $\xi_{(i,j)}$, is a function of the blueprint density. The indices (i, j) represent the vertical and horizontal position of the element respectively, i.e. element $i = 1$ is the layer on the baseplate. The vertical direction will be the printing direction in the following derivation. The elements will be printed if they are sufficiently supported. In the two dimensional case an element is considered to be sufficiently supported if it has three elements below, $n_s = 3$ and for a three dimensional case if it have nine elements below, $n_s = 9$. This results in that all elements supported by the baseplate are printable since it is always supported. Langelaar (2017) motivates this choice of the supporting area on that the self supporting angle for the considered processes is 45°. Using square elements for the two dimensional case and cubic elements for the three dimensional case provides the angle $\alpha = 45°$. This is illustrated in Figure 6.1 for the two dimensional case where an element, $e_{(i,j)}$, is fully supported.

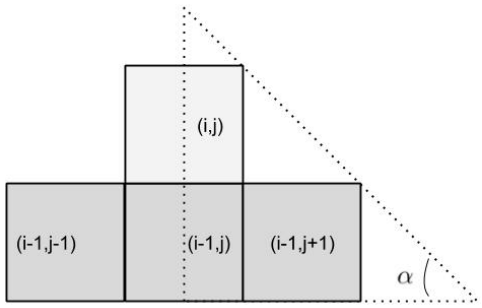

Figure 6.1: A fully supported element for the two dimensional case.

Elements located on the far left or far right edge will be taken into account for in the implementation as they are supported with two elements for the two dimensional case. This is done by adding an extra element with the value zero on each side. For elements $i \neq 1$, i.e. not on the baseplate, the element printed density is defined through that it can't be higher than the maximum printed density $\Xi_{(i,j)}$ in the supporting region. This is expressed as

$$\xi_{(i,j)} = min\left(\rho_{(i,j)}, \Xi_{(i,j)}\right) \tag{6.1}$$

$$\Xi_{(i,j)} = max\left(\xi_{(i-1,j-1)}, \xi_{(i-1,j)}, \xi_{(i-1,j+1)}\right) \tag{6.2}$$

As gradient information is essential in the topology optimization, Langelaar (2017) approximate the non-smooth functions in (6.1) and (6.2) as

$$s_{min}(\rho_{(i,j)}, \Xi_{(i,j)}) \equiv \frac{1}{2}\left(\rho_{(i,j)} + \Xi_{(i,j)} - \left(\left(\rho_{(i,j)} - \Xi_{(i,j)}\right)^2 + \varepsilon\right)^{\frac{1}{2}} + \sqrt{\varepsilon}\right) = \xi_{(i,j)} \tag{6.3}$$

$$s_{max}(\xi_{(i-1,j-1)}, \xi_{(i-1,j)}, \xi_{(i-1,j+1)}) \equiv \left(\xi^P_{(i-1,j-1)} + \xi^P_{(i-1,j)} + \xi^P_{(i-1,j+1)}\right)^{\frac{1}{Q}} = \Xi_{(i,j)} \tag{6.4}$$

$$\text{where} \qquad Q = P + \frac{\log(n_s)}{\log(\xi_0)}$$

The parameters P and ε in (6.3) and (6.4) controls the smoothness and accuracy of the approximation. If the parameters $\varepsilon \to 0$ and $P \to \infty$ the exact minimum and maximum operators are obtained. The default values for the parameters are set to $\varepsilon = 10^{-4}$, $P = 40$ and $\xi_0 = 0.5$. Consider an objective function to be minimized with a given constraint. The objective function depend on the printed geometry which in turn depend on the blue print design, $C(\boldsymbol{\xi}(\boldsymbol{\rho}))$. The chain rule provides

$$\frac{\partial C}{\partial \boldsymbol{\rho}} = \left[\frac{\partial C}{\partial \boldsymbol{\xi}} \frac{\partial \boldsymbol{\xi}}{\partial \tilde{\boldsymbol{\rho}}}\right] \frac{\partial \tilde{\boldsymbol{\rho}}}{\partial \boldsymbol{\rho}} \tag{6.5}$$

The filtered blueprint design field using a density filter is defined according to equation (3.32) and here becomes

$$\widetilde{\boldsymbol{\rho}}_e = \frac{\sum w_{e,i} v_i \rho_i}{\sum w_{e,i} v_i} \tag{6.6}$$

The first two parts in (6.5) are derived by combining (6.3) and (6.4), such that $s_{min}\left(\boldsymbol{\rho}_i, \boldsymbol{\xi}_{i-1}\right) - \boldsymbol{\xi}_i = 0$, and using this as the constraint equation. $\boldsymbol{\xi}_{i-1}$ is used because the printed density depend on the supporting region below. For efficiency the adjoint method is utilized. The augmented response of the objective function, $C(\boldsymbol{\xi}(\boldsymbol{\rho}))$, and the constraint function becomes

$$\widetilde{C} = C(\boldsymbol{\xi}(\tilde{\boldsymbol{\rho}})) + \sum_{i=1}^{n_i} \boldsymbol{\lambda}_i^T \left(s_{min}(\tilde{\boldsymbol{\rho}}_i, \boldsymbol{\xi}_{i-1}) - \boldsymbol{\xi}_i\right) \tag{6.7}$$

where $\boldsymbol{\lambda}_i$ are the adjoint vectors. At the first layer, right above the baseplate, differentiation of equation (6.7) and defining $\boldsymbol{\xi}_1 = s_{min,1} \equiv \tilde{\boldsymbol{\rho}}_1$ provides the following expression

$$\frac{\partial \widetilde{C}}{\partial \tilde{\boldsymbol{\rho}}_j} = \sum_{i=1}^{n_i} \left[\frac{\partial C}{\partial \boldsymbol{\xi}_i} \frac{\partial \boldsymbol{\xi}_i}{\partial \tilde{\boldsymbol{\rho}}_j} + \boldsymbol{\lambda}_i^T \left(\frac{\partial s_{min,i}}{\partial \tilde{\boldsymbol{\rho}}_j} \delta_{ij} + \frac{\partial s_{min,i}}{\partial \boldsymbol{\xi}_{i-1}} \frac{\partial \boldsymbol{\xi}_{i-1}}{\partial \tilde{\boldsymbol{\rho}}_j} - \frac{\partial \boldsymbol{\xi}_i}{\partial \tilde{\boldsymbol{\rho}}_j} \right) \right] \tag{6.8}$$

The printed densities only depend on the blueprint density and the result of this is $\frac{\partial \boldsymbol{\xi}_i}{\partial \tilde{\boldsymbol{\rho}}_j} = 0$ for $i < j$. Using the constraint mentioned above, moving terms with $i = j$ outside of the summation and writing the last term in the summation as a separate sum provides

$$\frac{\partial \widetilde{C}}{\partial \tilde{\boldsymbol{\rho}}_j} = \frac{\partial C}{\partial \boldsymbol{\xi}_j} \frac{\partial \boldsymbol{\xi}_j}{\partial \tilde{\boldsymbol{\rho}}_j} + \sum_{i=j+1}^{n_i} \left(\frac{\partial C}{\partial \boldsymbol{\xi}_i} - \boldsymbol{\lambda}_i \right) \frac{\partial \boldsymbol{\xi}_i}{\partial \tilde{\boldsymbol{\rho}}_j} + \sum_{i=j+1}^{n_i} \left(\boldsymbol{\lambda}_i^T \frac{\partial s_{min,i}}{\partial \boldsymbol{\xi}_{i-1}} \frac{\partial \boldsymbol{\xi}_{i-1}}{\partial \tilde{\boldsymbol{\rho}}_j} \right) \tag{6.9}$$

From the second summation the first term $i = j + 1$ is moved outside of the summation. The remaining is reindexed and the last term in the first sum is moved outside of the summation making the two sums regain the same limits. Again using the constraint mentioned above, equation (6.9) becomes

$$\frac{\partial \widetilde{C}}{\partial \tilde{\boldsymbol{\rho}}_j} = \left(\frac{\partial C}{\partial \boldsymbol{\xi}_j} + \boldsymbol{\lambda}_{j+1}^T \frac{\partial s_{min,j+1}}{\partial \boldsymbol{\xi}_j} \right) \frac{\partial s_{min,j}}{\partial \tilde{\boldsymbol{\rho}}_j} + \left(\frac{\partial C}{\partial \boldsymbol{\xi}_{ni}} - \boldsymbol{\lambda}_{n_i}^T \right) \frac{\partial \boldsymbol{\xi}_{n_i}}{\partial \tilde{\boldsymbol{\rho}}_j} + \sum_{i=j+1}^{n_i - 1} \left(\frac{\partial C}{\partial \boldsymbol{\xi}_i} - \boldsymbol{\lambda}_i^T + \boldsymbol{\lambda}_{i+1}^T \frac{\partial s_{min,i+1}}{\partial \boldsymbol{\xi}_i} \right) \frac{\partial \boldsymbol{\xi}_i}{\partial \tilde{\boldsymbol{\rho}}_j} \tag{6.10}$$

Equation (6.10) holds for $1 \leq j \leq n_i$ and in order to simplify the calculations $\boldsymbol{\lambda}_i$ and $\boldsymbol{\lambda}_{n_i}$ are chosen in the following manner

$$\boldsymbol{\lambda}_j^T = \frac{\partial C}{\partial \boldsymbol{\xi}_j} + \boldsymbol{\lambda}_{j+1}^T \frac{\partial s_{min,j+1}}{\partial \boldsymbol{\xi}_j} \qquad \text{for} \qquad 1 \leq j < n_i \qquad \boldsymbol{\lambda}_{n_i}^T = \frac{\partial C}{\partial \boldsymbol{\xi}_{n_i}} \tag{6.11}$$

The multipliers above avoids calculations of the term $\frac{\partial \boldsymbol{\xi}_i}{\partial \tilde{\boldsymbol{\rho}}}$. The term $\frac{\partial C}{\partial \boldsymbol{\xi}_j}$ will be similar to the first part in (3.34) but with respect to the printed density, ξ_j, if the SIMP method is used. Equation(6.10) together with the multipliers in (6.11) becomes

$$\frac{\partial C}{\partial \tilde{\boldsymbol{\rho}}_j} = \frac{\partial \widetilde{C}}{\partial \tilde{\boldsymbol{\rho}}_j} = \left(\frac{\partial C}{\partial \boldsymbol{\xi}_j} + \boldsymbol{\lambda}_{j+1}^T \frac{\partial s_{min,j+1}}{\partial \boldsymbol{\xi}_j} \right) \frac{\partial s_{min,j}}{\partial \tilde{\boldsymbol{\rho}}_j} = \boldsymbol{\lambda}_j^T \frac{\partial s_{min,j}}{\partial \tilde{\boldsymbol{\rho}}_j} \tag{6.12}$$

It can be observed that each multiplier depend on the layer above. This results in that the algorithm start at the top layer and moves down. The following expressions are used when calculating the derivatives of s_{min} in (6.12) and are derived using (6.3), and (6.4).

$$\frac{\partial s_{min}(x, \Xi)}{\partial \rho} = \frac{1}{2} \left(1 - (\rho - \Xi) \left((\rho - \Xi)^2 + \varepsilon \right)^{-\frac{1}{2}} \right) \tag{6.13}$$

$$\frac{\partial s_{min}}{\partial \xi} = \frac{\partial s_{min}}{\partial \Xi} \frac{\partial \Xi}{\partial \xi} \qquad \text{where} \qquad \begin{cases} \frac{\partial s_{min}(\rho, \Xi)}{\partial \Xi} = \frac{1}{2} \left(1 + (\rho - \Xi) \left((\rho - \Xi)^2 + \varepsilon \right)^{-\frac{1}{2}} \right) \\ \frac{\partial \Xi(\xi_1, \xi_2, \xi_3)}{\partial \xi_i} = \frac{P \xi_i^{P-1}}{Q} \left(\sum_{k=1}^{n_s} \xi_k^P \right)^{\frac{1}{Q} - 1} \end{cases} \tag{6.14}$$

The last part in (6.5) is the same expression calculated in the sensitivity analysis for the density filter in Section 3.4, i.e. the second part in (3.34), and is derived from equation

(6.6). With the considered method four different printing directions can be examined due to the definition of the supported region. These are depicted in Figure 6.2.

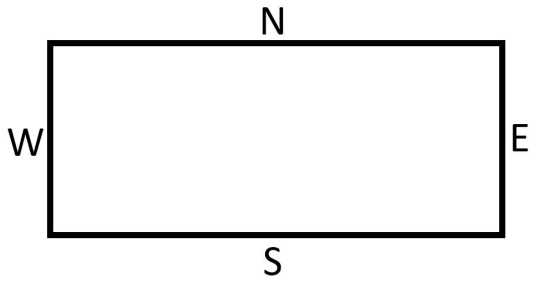

Figure 6.2: Baseplates for the additive manufacturing filter.

6.2 Performance and Result

The additive manufacturing filter is provided by Langelaar (2017) and is prepared for integration with the 88-line topology optimization code by Andreassen et al. (2011). The topology optimization is performed on a two dimensional MBB beam, geometry and boundary conditions depicted in Figure 6.3.

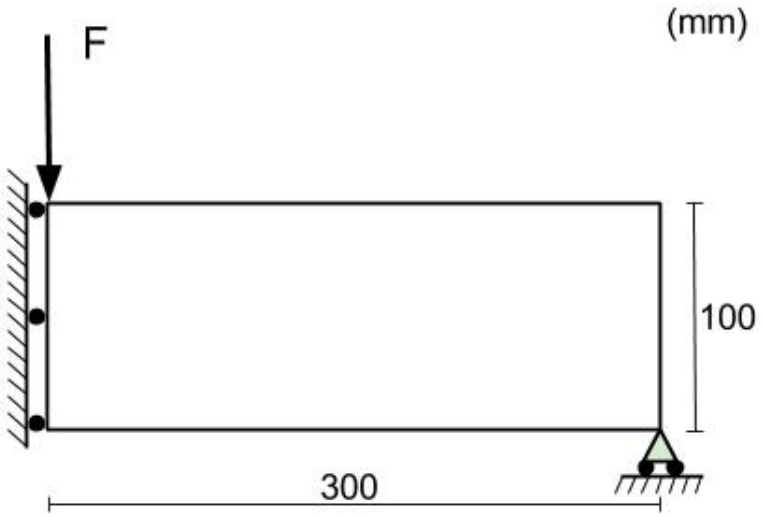

Figure 6.3: Illustration of the geometry and boundary conditions.

The topology optimization code by Andreassen et al. (2011) is solved with the OC method using the modified SIMP, $E_{min} = 10^{-9}$ and $E_0 = 1$, and a density filter. The reference cases is depicted in Figure 6.4 for two different meshes, 14x42 and 40x120 elements. Algorithmic parameters used in the coarse mesh are $\alpha = 1$, $p = 3$, $V_{max} = 0.4V_{box}$ and $R = 1.0*$(element side length). Algorithmic parameters used in the fine mesh are $\alpha = 1$, $p = 3$, $V_{max} = 0.4V_{box}$ and $R = 1.0 * \sqrt{\frac{\text{number of elements fine mesh}}{\text{number of elements coarse mesh}}} *$(element side length)

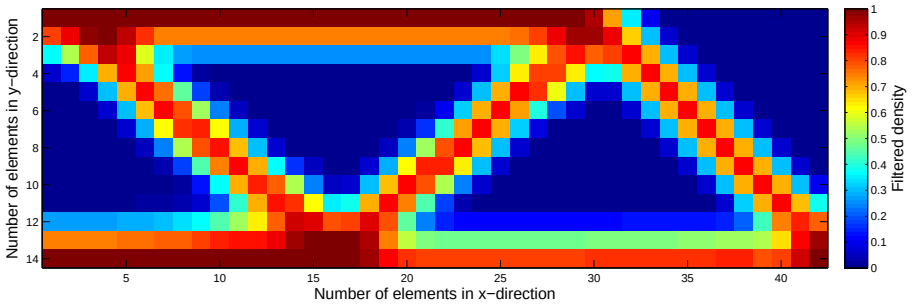

(a) Coarse mesh, 14x42 elements.

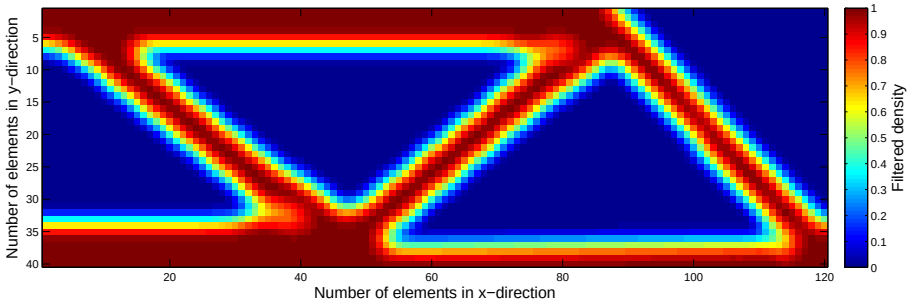

(b) Fine mesh, 40x120 elements.

Figure 6.4: Topology optimization solved using the modified SIMP method and a density filter.

The additive manufacturing filter is applied in Figure 6.5 for the different directions N, S, E, W. It is clear that the different orientations provide different results. To compare the performance of the different results the relative compliance between the reference and respective orientation is calculated. The relative compliance is 139%, 127%, 115% and 99% respectively. In this case the W-direction becomes the most favourable due to that the compliance does not increase and the N-direction becomes the least favourable with the highest increase in compliance. The N-direction and the S-direction contains areas with intermediate densities which the E-direction and W-direction do not to the same extent.

The result of the additive manufacturing filter on a finer mesh is depicted in Figure 6.6. The relative compliance comparing with the reference is 134%, 116%, 109% and 98% respectively. The W-direction provides the best result in performance comparing the relative density and the N-direction the worst with the highest increase of the compliance. For the fine mesh mainly the N-direction contain supports with intermediate density. However, intermediate density regions can be observed in the E-direction and S-direction as well but not in the W-direction in the same extent. Due to the nature of the density filter, i.e. the smooth transitions between material and void, regions that are not affected by the additive manufacturing filter will contain intermediate density.

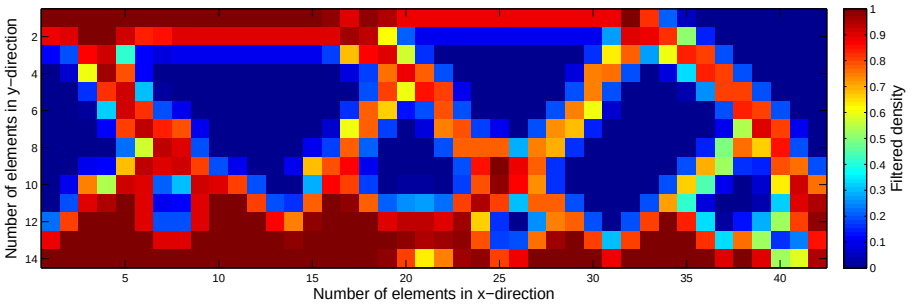

(a) Coarse mesh, N-direction. $\frac{C}{C_{ref}} = 1.39$

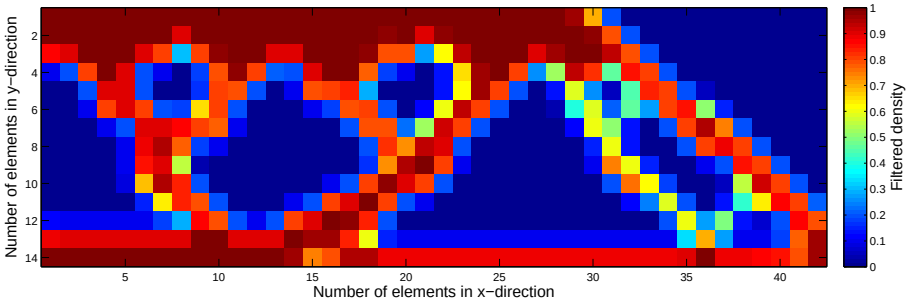

(b) Coarse mesh, S-direction. $\frac{C}{C_{ref}} = 1.27$

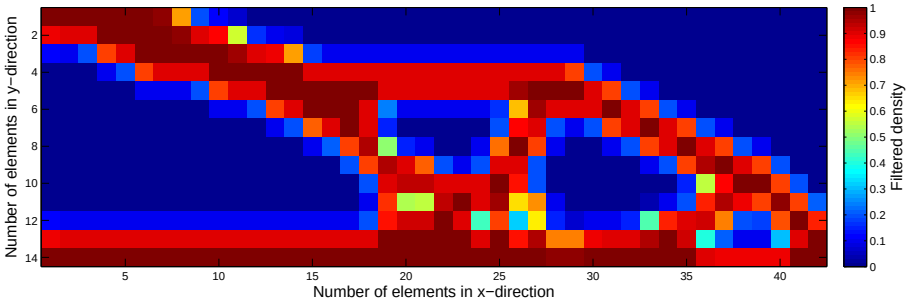

(c) Coarse mesh, E-direction. $\frac{C}{C_{ref}} = 1.15$

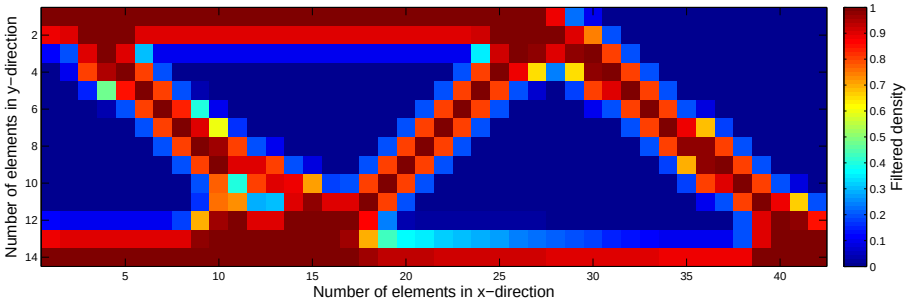

(d) Coarse mesh, W-direction. $\frac{C}{C_{ref}} = 0.99$

Figure 6.5: Additive manufacturing filter by Langelaar (2017) applied on the coarse mesh.

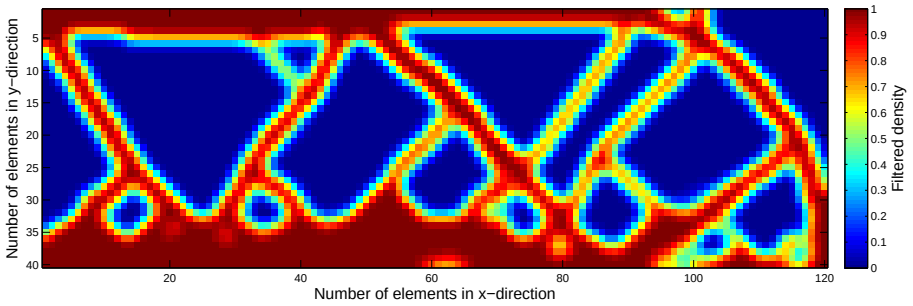

(a) Fine mesh, N-direction. $\frac{C}{C_{ref}} = 1.34$

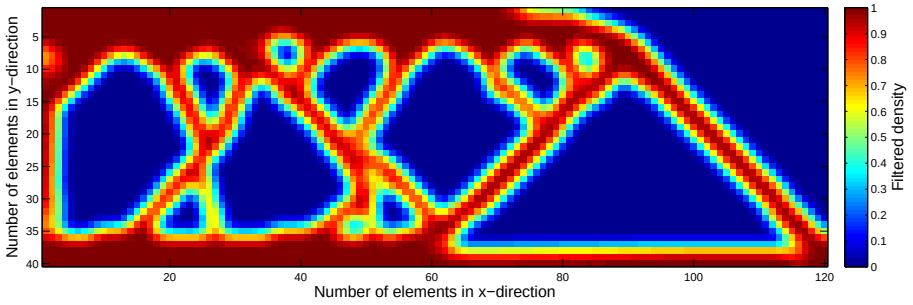

(b) Fine mesh, S-direction. $\frac{C}{C_{ref}} = 1.16$

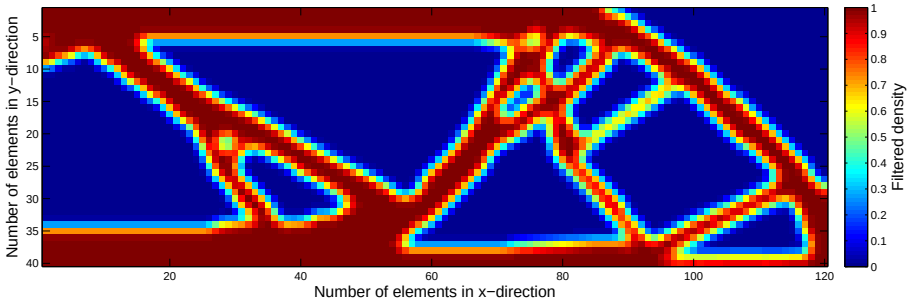

(c) Fine mesh, E-direction. $\frac{C}{C_{ref}} = 1.09$

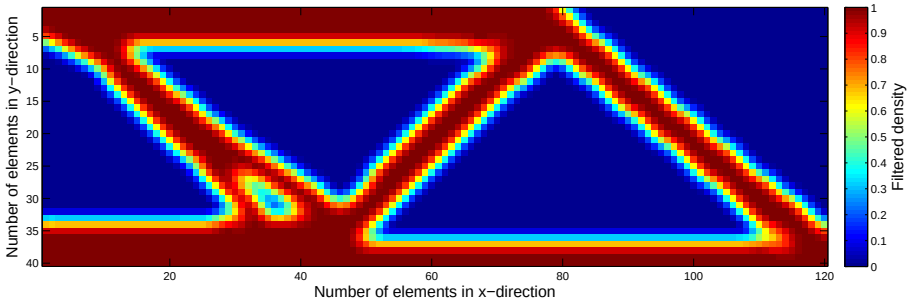

(d) Fine mesh, W-direction. $\frac{C}{C_{ref}} = 0.99$

Figure 6.6: Additive manufacturing filter by Langelaar (2017) applied on the fine mesh.

A different topology can be observed for each direction comparing with the topology in the coarse mesh. This is probably the effect of how an element is distinguished to be supported. A compiled result of the relative compliance for the two meshes is presented in Table 6.1. The W-direction provides the best result and the N-direction the worst result regarding the relative compliance in both meshes. The relative compliance for the

W-direction is less than for the reference. This could be due to that the reference case is a local optimum or the small intermediate region in the W-direction affecting the stiffness. The choice of the R-parameter also affect the compliance and it might not be chosen to the optimal value for the reference case. It should also be noticed that some bars meets the side of other bars, for example in the E-direction. This would cause a bending moment which would normally not be preferable in the optimal case.

Baseplate	Coarse Mesh $\frac{C}{C_{ref}}$	Fine Mesh $\frac{C}{C_{ref}}$
N	139%	134%
S	127%	116%
E	115%	109%
W	99%	98%

Table 6.1: Relative compliance for the method by Langelaar (2017)

The biggest advantage with the method by Langelaar (2017), except that the models becomes printable regarding the overhang constraint, is the computational time. Figure 6.7 presents a computational time curve for the reference model and all printing directions. The elements in the y-direction is a third of the elements in the x-direction. The filter radius R increases with the same fraction as the elements in each direction increases. The maximum amount of iterations in the algorithm is set to 200 iterations. For the finest mesh all models including the reference reach the maximum amount of optimization iterations. In order to decrease the computational time even more another algorithm could be used. The OC optimizer by Andreassen et al. (2011) contains an inner loop where the volume constraint is calculated a number of times which means the additive manufacturing filter is called the same amount of times. Using for instance the method of moving asymptotes, MMA, by Svanberg (1987) only one call of the additive manufacturing filter would be necessary per iteration which would decrease the computational time.

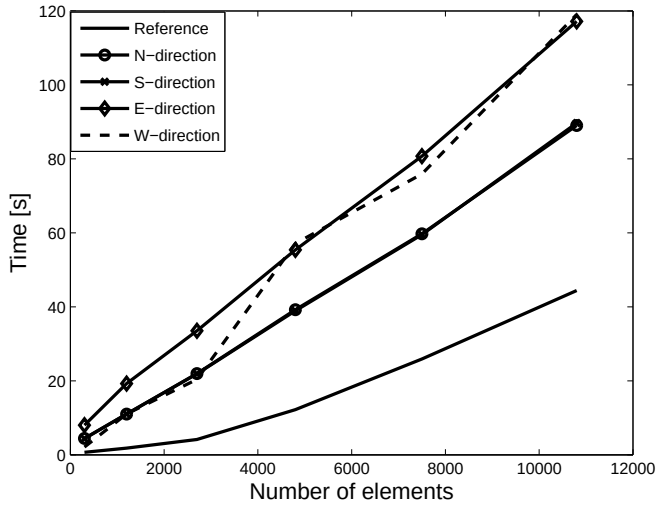

Figure 6.7: Computational time curve for the method by Langelaar (2017).

As mentioned before the printing direction plays a crucial part on which surfaces are print-

able. This is very easily verified when comparing the relative compliance and topologies for the different directions retrieved with the additive manufacturing filter. This leads to a major disadvantage of this method where the additive manufacturing filter requires the print direction to be axiparallel to the coordinate axis. This might be circumvented through isoparametric formulation and element mapping, but would complicate the calculations and consequently the computation time would increase. The same constraint, i.e. the support region tied to the element discretization, leads to the next big disadvantage. The self supporting angle is tied to the aspect ratio of the elements. In order to analyze an angle different from 45° the ratio between the element sides need to be changed. The nature of the additive manufacturing filter lead to mesh dependence which is not desired. To overcome this the definition of the supporting region need to be changed. The density in an element should not only be defined by the density in adjacent elements. These disadvantages should be further addressed to increase the usage of the filter. Finally, the method requires information about neighbour elements which for fine meshes or complex domains and geometries become very difficult to obtain thus it is an expensive operation. During parallel computing, where the design domain is decomposed into partitions, the complexity of problem increases further.

Chapter 7

Density Gradient Method

The disadvantages regarding that the critical angle being tied to the aspect ratio of the element, or the axiparallel print direction in the additive manufacturing filter by Langelaar (2017) could be further addressed using the same method. However, in order to address the constraint with the requirement of neighbour elements the entire formulation needs to be changed. As mentioned before the density filter as a solution of Helmholtz PDE by Lazarov and Sigmund (2011) does not require this sort of information about the neighbour elements, thus could become more advantageous to use for a finer or more complicated mesh.

7.1 Density Gradient

The same idea as when calculating the temperature gradient in two dimensional heat flow is used when calculating the density gradient. For a four-node rectangular element the boundaries must be parallel to the coordinate system. In order to get a more generalized formulation the density gradient is derived for a four-node isoparametric quadrilateral element and the mapping is illustrated in Figure 7.1.

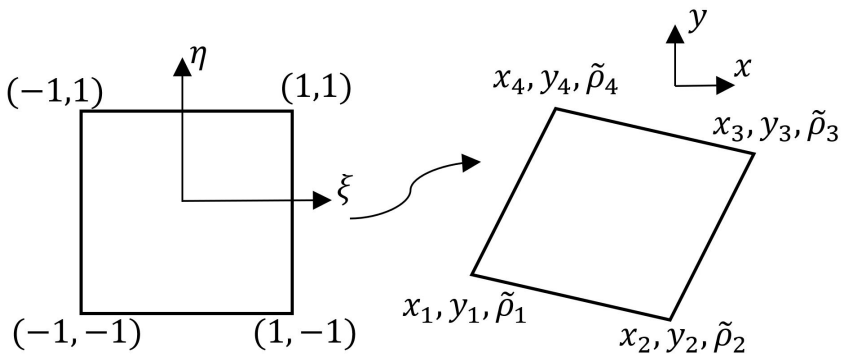

Figure 7.1: Illustation of an element mapping.

The density gradient in two dimensions is

$$\nabla\tilde{\rho} = \begin{bmatrix} \frac{\partial\tilde{\rho}}{\partial x} \\ \frac{\partial\tilde{\rho}}{\partial y} \end{bmatrix} \tag{7.1}$$

The shape functions for a four-node isoparametric quadrilateral element are

$$\begin{aligned} N_1^e &= \frac{1}{4}(\xi-1)(\eta-1) \\ N_2^e &= -\frac{1}{4}(\xi+1)(\eta-1) \\ N_3^e &= \frac{1}{4}(\xi+1)(\eta+1) \\ N_4^e &= -\frac{1}{4}(\xi-1)(\eta+1) \end{aligned} \tag{7.2}$$

The mapping between the coordinate systems is obtained through

$$x = x(\xi,\eta) = \boldsymbol{N}^e(\xi,\eta)\boldsymbol{x}^e \qquad y = y(\xi,\eta) = \boldsymbol{N}^e(\xi,\eta)\boldsymbol{y}^e \tag{7.3}$$

where

$$\boldsymbol{N}^e(\xi,\eta) = \begin{bmatrix} N_1^e & N_2^e & N_3^e & N_4^e \end{bmatrix}, \qquad \boldsymbol{x}^e = \begin{bmatrix} x_1 \\ x_2 \\ x_3 \\ x_4 \end{bmatrix}, \qquad \boldsymbol{y}^e = \begin{bmatrix} y_1 \\ y_2 \\ y_3 \\ y_4 \end{bmatrix} \tag{7.4}$$

The approximation of the density is

$$\tilde{\rho} = \tilde{\rho}(\xi,\eta) = \boldsymbol{N}^e(\xi,\eta)\tilde{\boldsymbol{\rho}} \qquad \text{where} \qquad \tilde{\boldsymbol{\rho}} = \begin{bmatrix} \tilde{\rho}_1 & \tilde{\rho}_2 & \tilde{\rho}_3 & \tilde{\rho}_4 \end{bmatrix} \tag{7.5}$$

Equation (7.1) can be rewritten using the approximation in (7.5) and becomes

$$\nabla\tilde{\rho} = \begin{bmatrix} \frac{\partial \boldsymbol{N}^e}{\partial x} \\ \frac{\partial \boldsymbol{N}^e}{\partial y} \end{bmatrix} \tilde{\boldsymbol{\rho}} = (\boldsymbol{J}^T)^{-1} \begin{bmatrix} \frac{\partial \boldsymbol{N}^e}{\partial \xi} \\ \frac{\partial \boldsymbol{N}^e}{\partial \eta} \end{bmatrix} \tilde{\boldsymbol{\rho}} \qquad \text{where} \qquad \boldsymbol{J} = \begin{bmatrix} \frac{\partial x}{\partial \xi} & \frac{\partial x}{\partial \eta} \\ \frac{\partial y}{\partial \xi} & \frac{\partial y}{\partial \eta} \end{bmatrix} \tag{7.6}$$

7.2 Additive Manufacturing Filter

In Figure 7.2 the gradient vector and the normal to the baseplate are illustrated. The gradient vector represents the gradient of the filtered density variables. Using the definition of the scalar product, in equation (7.7), the angle between the normal to the baseplate and the density gradient can be calculated

$$\theta = \arccos\left(\frac{\boldsymbol{v}^T\nabla\tilde{\rho}}{\|\boldsymbol{v}\|\,\|\nabla\tilde{\rho}\|}\right) \tag{7.7}$$

If using the fact that the normal to the baseplate, $\boldsymbol{v}$, is $[0,1,0]$, the elements with angles less than the critical angle can be determined. If an angle θ_0 is defined as the critical angle the angles smaller than this is at risk, i.e. $\theta \leq \theta_0$ interfere with the constraint. This is illustrated in Figure 7.2 where the green line represents the smallest allowed angle and the red line represents an angle smaller than the minimum allowed angle.

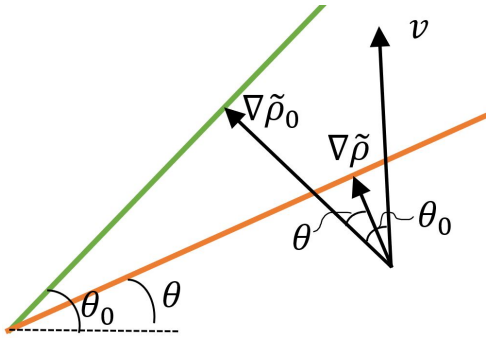

Figure 7.2: Illustration of the density gradient constraint.

7.2.1 Formulation

In the same manner as when using the energy balance (strong form) to obtain the minimization of the functional for heat conduction and the principle of virtual temperatures the PDE filter could be examined.

$$-\nabla^T \boldsymbol{K}_d \nabla\tilde{\rho} + \tilde{\rho} = \rho \tag{7.8}$$

The strong form of (7.8) is

$$div(-\boldsymbol{K}_d \nabla\tilde{\rho}) + \tilde{\rho} = \rho \tag{7.9}$$

The potential associated with (7.9)

$$\Pi(\tilde{\rho}) = \int_V \frac{1}{2}(\nabla\tilde{\rho})^T \boldsymbol{K}_d \nabla\tilde{\rho} dV + \int_V \frac{1}{2}(\rho - \tilde{\rho})^2 dV - \int_{\partial V} \tilde{\rho} q_n dS \tag{7.10}$$

where the last part vanishes since $q_n = 0$ on ∂S. Moreover, if the function $w = \frac{1}{2}\nabla\tilde{\rho}^T \boldsymbol{K}_d \nabla\tilde{\rho}$ is defined, where $\boldsymbol{K}_d$ is positive definite, the functional in (7.10) becomes

$$\Pi(\tilde{\rho}) = \int_V w(\nabla\tilde{\rho}) dV + \int_V \frac{1}{2}(\rho - \tilde{\rho})^2 dV \tag{7.11}$$

and the minimization of the functional is

$$\delta\Pi = \int_V \frac{\partial w}{\partial \nabla\tilde{\rho}} \delta(\nabla\tilde{\rho}) dV - \int_V (\rho - \tilde{\rho}) \delta\tilde{\rho} dV \tag{7.12}$$

Upon using $q_i = \left(\frac{\partial w}{\partial \nabla\tilde{\rho}}\right)$, equation (7.12) can be expressed as

$$\delta\Pi = \int_V q_i \frac{\partial}{\partial x_i}(\delta\tilde{\rho}) dV - \int_V (\rho - \tilde{\rho}) \delta\tilde{\rho} dV \tag{7.13}$$

Making use of $\int_V (q_i \delta\tilde{\rho})_{,i} dV = \int_{\partial V} q_i \delta\tilde{\rho} n_i dS = 0$ where the last equality holds due to q_i=0 provides after some calculation the weak form

$$\int_V -v_{,i} q_i dV + \int_V v\tilde{\rho} dV = \int_V v\rho \tag{7.14}$$

For the FE-formulation of the weak form of the filter equation (7.14) the following notations is used $\tilde{\rho}_e = \boldsymbol{N}_e \tilde{\boldsymbol{\rho}}$, $\boldsymbol{v} = \boldsymbol{N}_e \boldsymbol{c}$, $\nabla v = \boldsymbol{B}_e \boldsymbol{c}$ and equation (7.14) takes the form

$$\int_V \boldsymbol{B}^T \boldsymbol{q} dV + \int_V \boldsymbol{N}^T \boldsymbol{N} dV \tilde{\boldsymbol{\rho}} = \int_V \boldsymbol{N}^T dV \boldsymbol{\rho} \tag{7.15}$$

With $\boldsymbol{M} = \int_V \boldsymbol{N}^T \boldsymbol{N} dV$ and $\boldsymbol{T} = \int_V \boldsymbol{N}^T dV$ equation (7.15) becomes

$$\boldsymbol{R}(\tilde{\boldsymbol{\rho}}, \boldsymbol{\rho}) = \int_V \boldsymbol{B}^T \boldsymbol{q} dV + \boldsymbol{M}\tilde{\boldsymbol{\rho}} - \boldsymbol{T}\boldsymbol{\rho} = \boldsymbol{0} \tag{7.16}$$

In order to change the nature of the filter the function $w(\nabla\tilde{\rho})$ could be changed, for instance to a non-linear function.

To solve this system of potentially non-linear equations Newton Raphson's method could be used. Newton Raphson's method makes use of the known solution from the previous iteration, n, to solve the current iteration, $n+1$. Taylor's first order approximation of the residual function is

$$\boldsymbol{R}^{n+1}(\tilde{\boldsymbol{\rho}}^{n+1}, \boldsymbol{\rho}) = \boldsymbol{R}^n(\tilde{\boldsymbol{\rho}}^n, \boldsymbol{\rho}) + \frac{\partial \boldsymbol{R}^n(\tilde{\boldsymbol{\rho}}^n, \boldsymbol{\rho})}{\partial \tilde{\boldsymbol{\rho}}^n} \left(\tilde{\boldsymbol{\rho}}^{n+1} - \tilde{\boldsymbol{\rho}}^n\right) = \boldsymbol{0} \tag{7.17}$$

Using that the residual in the updated state, $\boldsymbol{R}^{n+1}(\tilde{\boldsymbol{\rho}}^{n+1}, \boldsymbol{\rho})$, is small compared with the previous state , $\boldsymbol{R}^n(\tilde{\boldsymbol{\rho}}^n, \boldsymbol{\rho})$, the filtered densities from the current iteration can be solved from

$$\tilde{\boldsymbol{\rho}}^{n+1} = \tilde{\boldsymbol{\rho}}^n - \left(\frac{\partial \boldsymbol{R}^n(\tilde{\boldsymbol{\rho}}^n, \boldsymbol{\rho})}{\partial \tilde{\boldsymbol{\rho}}^n}\right)^{-1} \boldsymbol{R}^n(\tilde{\boldsymbol{\rho}}^n, \boldsymbol{\rho}) \tag{7.18}$$

The residual function can be updated using the new $\tilde{\boldsymbol{\rho}}^{n+1}$. If $\boldsymbol{R}^{n+1}(\tilde{\boldsymbol{\rho}}^{n+1}, \boldsymbol{\rho}) > tolerance$ the next iteration, $n = n+1$, will be calculated. The derivative of the filter function with respect to the filtered density, $\tilde{\boldsymbol{\rho}}$, needs to be calculated and becomes

$$\frac{\partial \boldsymbol{R}(\tilde{\boldsymbol{\rho}}, \boldsymbol{\rho})}{\partial \tilde{\boldsymbol{\rho}}} = \int_V \boldsymbol{B}^T \frac{\partial \boldsymbol{q}}{\partial \tilde{\boldsymbol{\rho}}} dV + \boldsymbol{M} = \boldsymbol{0} \tag{7.19}$$

With $\boldsymbol{K}_d = \frac{\partial q_i}{\partial \nabla \tilde{\boldsymbol{\rho}}}$ equation (7.19) becomes

$$\frac{\partial \boldsymbol{R}(\tilde{\boldsymbol{\rho}}, \boldsymbol{\rho})}{\partial \tilde{\boldsymbol{\rho}}} = \int_V \boldsymbol{B}^T \boldsymbol{K}_d \boldsymbol{B} dV + \boldsymbol{M} = \boldsymbol{0} \tag{7.20}$$

7.2.2 Sensitivity Analysis

The filter is expressed as

$$\boldsymbol{R}(\tilde{\boldsymbol{\rho}}, \boldsymbol{\rho}) = \boldsymbol{0} \tag{7.21}$$

The sensitivity analysis is performed using the adjoint method. The objective function, g, including the non linear filter can be written as

$$g = \boldsymbol{F}^T \boldsymbol{u}(\boldsymbol{\rho}) + \boldsymbol{\lambda}^T (\boldsymbol{K}\boldsymbol{u} - \boldsymbol{F}) + \boldsymbol{\Lambda}^T \boldsymbol{R}(\tilde{\boldsymbol{\rho}}, \boldsymbol{\rho}) \tag{7.22}$$

where $\boldsymbol{\lambda}$ is the linear Lagrange multiplier and $\boldsymbol{\Lambda}$ is the non linear Lagrange multiplier. Differentiation of (7.22) becomes

$$\frac{\partial g}{\partial \boldsymbol{\rho}} = \boldsymbol{F}^T \frac{\partial \boldsymbol{u}}{\partial \boldsymbol{\rho}} + \boldsymbol{\lambda}^T \left[\frac{\partial \boldsymbol{K}}{\partial \tilde{\boldsymbol{\rho}}} \frac{\partial \tilde{\boldsymbol{\rho}}}{\partial \boldsymbol{\rho}} \boldsymbol{u} + \boldsymbol{K} \frac{\partial \boldsymbol{u}}{\partial \boldsymbol{\rho}} \right] + \boldsymbol{\Lambda}^T \left[\frac{\partial \boldsymbol{R}(\tilde{\boldsymbol{\rho}}, \boldsymbol{\rho})}{\partial \tilde{\boldsymbol{\rho}}} \frac{\partial \tilde{\boldsymbol{\rho}}}{\partial \boldsymbol{\rho}} + \frac{\partial \boldsymbol{R}(\tilde{\boldsymbol{\rho}}, \boldsymbol{\rho})}{\partial \boldsymbol{\rho}} \right] \tag{7.23}$$

In order to simplify the expression in (7.23) and to avoid calculations of the terms $\frac{\partial \boldsymbol{u}}{\partial \boldsymbol{\rho}}$ and $\frac{\partial \tilde{\boldsymbol{\rho}}}{\partial \boldsymbol{\rho}}$ it is rewritten to

$$\frac{\partial g}{\partial \boldsymbol{\rho}} = \underbrace{\left[\boldsymbol{F}^T + \boldsymbol{\lambda}^T \boldsymbol{K} \right]}_{=\mathbf{0}} \frac{\partial \boldsymbol{u}}{\partial \boldsymbol{\rho}} + \underbrace{\left[\boldsymbol{\lambda}^T \frac{\partial \boldsymbol{K}}{\partial \tilde{\boldsymbol{\rho}}} \boldsymbol{u} + \boldsymbol{\Lambda}^T \frac{\partial \boldsymbol{R}(\tilde{\boldsymbol{\rho}}, \boldsymbol{\rho})}{\partial \tilde{\boldsymbol{\rho}}} \right]}_{=\mathbf{0}} \frac{\partial \tilde{\boldsymbol{\rho}}}{\partial \boldsymbol{\rho}} + \boldsymbol{\Lambda}^T \frac{\partial \boldsymbol{R}(\tilde{\boldsymbol{\rho}}, \boldsymbol{\rho})}{\partial \boldsymbol{\rho}} \tag{7.24}$$

Using the equilibrium equation the first part provide the linear multiplier

$$\boldsymbol{F}^T + \boldsymbol{\lambda}^T \boldsymbol{K} = \mathbf{0} \quad \Longrightarrow \quad \boldsymbol{\lambda}^T = -\boldsymbol{u}^T \tag{7.25}$$

Using the linear multiplier in the second part provides the non linear multiplier

$$\boldsymbol{\lambda}^T \frac{\partial \boldsymbol{K}}{\partial \tilde{\boldsymbol{\rho}}} \boldsymbol{u} + \boldsymbol{\Lambda}^T \frac{\partial \boldsymbol{R}(\tilde{\boldsymbol{\rho}}, \boldsymbol{\rho})}{\partial \tilde{\boldsymbol{\rho}}} = \mathbf{0}$$

$$\Longrightarrow \quad -\boldsymbol{u}^T \frac{\partial \boldsymbol{K}}{\partial \tilde{\boldsymbol{\rho}}} \boldsymbol{u} + \boldsymbol{\Lambda}^T \frac{\partial \boldsymbol{R}(\tilde{\boldsymbol{\rho}}, \boldsymbol{\rho})}{\partial \tilde{\boldsymbol{\rho}}} = \mathbf{0}$$

$$\Longleftrightarrow \quad \boldsymbol{\Lambda}^T = \boldsymbol{u}^T \frac{\partial \boldsymbol{K}}{\partial \tilde{\boldsymbol{\rho}}} \boldsymbol{u} \left(\frac{\partial \boldsymbol{R}(\tilde{\boldsymbol{\rho}}, \boldsymbol{\rho})}{\partial \tilde{\boldsymbol{\rho}}} \right)^{-1} \tag{7.26}$$

Now the sensitivity can be calculated and the only remaining part is the third part thus it becomes

$$\frac{\partial g}{\partial \boldsymbol{\rho}} = \boldsymbol{\Lambda}^T \frac{\partial \boldsymbol{R}(\tilde{\boldsymbol{\rho}}, \boldsymbol{\rho})}{\partial \boldsymbol{\rho}} \tag{7.27}$$

For the conventional filter the function $w(\nabla \tilde{\rho})$ is

$$w = \frac{1}{2} \nabla \tilde{\boldsymbol{\rho}}^T \boldsymbol{K}_d \nabla \tilde{\boldsymbol{\rho}} \tag{7.28}$$

The derivatives become

$$q_i = \frac{\partial w}{\partial \nabla \tilde{\boldsymbol{\rho}}} = \boldsymbol{K}_d \nabla \tilde{\boldsymbol{\rho}} = r^2 \boldsymbol{I} \nabla \tilde{\boldsymbol{\rho}} \tag{7.29}$$

$$\boldsymbol{K}_d = \frac{\partial q_i}{\partial \nabla \tilde{\boldsymbol{\rho}}} = \frac{\partial^2 w}{\partial \nabla \tilde{\boldsymbol{\rho}}^2} = r^2 \boldsymbol{I} \tag{7.30}$$

The sensitivity using these functions become

$$\frac{\partial g}{\partial \rho} = \boldsymbol{\Lambda}^T \frac{\partial \boldsymbol{R}(\tilde{\boldsymbol{\rho}}, \rho)}{\partial \rho} = -\boldsymbol{u}^T \frac{\partial \boldsymbol{K}}{\partial \tilde{\boldsymbol{\rho}}} \boldsymbol{u} (\boldsymbol{K} + \boldsymbol{M})^{-1} \boldsymbol{T} \tag{7.31}$$

where $\boldsymbol{K} = \int_V \boldsymbol{B}^T \boldsymbol{K}_d \boldsymbol{B} dV$, $\boldsymbol{M} = \int_V \boldsymbol{N}^T \boldsymbol{N} dV$ and $\boldsymbol{T} = \int_V \boldsymbol{N}^T dV$. When comparing the expression in (7.31) with (3.45) and (3.46) in the regular density filter as a solution of Helmholtz PDE these are the same, i.e. .

7.2.3 The Function $w(\nabla\tilde{\rho})$

As mentioned before the nature of the filter could be changed by changing the function $w(\nabla\tilde{\rho})$. It is dependent on the gradient of the filtered densities and using the definition of the scalar product

$$cos(\theta) = \left(\frac{\boldsymbol{v}^T \nabla\tilde{\rho}}{||\boldsymbol{v}||\,||\nabla\tilde{\boldsymbol{\rho}}||} \right) \tag{7.32}$$

provides an expression depending on the gradient of the filtered densities and a vector, $\boldsymbol{v}^T = [x, y, z]$, describing a direction. An expression using the scalar product with a function that reacts on for instance the critical angle and penalize angles below 45° could be formed. The function should almost act as a step function where if the angle between the gradient and the baseplate is below a certain critical angle it should be penalized. To get a smooth continuous function the following expression could be used

$$w(\nabla\tilde{\rho}) = r^2\left[\arctan(z) + e^z\right] \qquad \text{where} \qquad z = \beta\left[c + \left(\frac{\boldsymbol{v}\nabla\tilde{\rho}}{||\boldsymbol{v}||\,||\nabla\tilde{\rho}||}\right)\right] \tag{7.33}$$

where β and c are constants used to control the position and rate of the function could be chosen and the parameter r^2 scales down the functions and could be related to the size of the elements. The derivatives becomes

$$q_i = \frac{\partial w(\nabla\tilde{\rho})}{\partial\nabla\tilde{\rho}} = r^3\left[\frac{1}{1+z^2}\frac{\partial z}{\partial\nabla\tilde{\rho}} + e^z\frac{\partial z}{\partial\nabla\tilde{\rho}}\right] \tag{7.34}$$

$$\begin{aligned}\boldsymbol{K}_d = \frac{\partial q_i}{\partial\nabla\tilde{\rho}} = \frac{\partial^2 w(\nabla\tilde{\rho})}{\partial\nabla\tilde{\rho}^2} = r^3\Bigg[&\frac{1}{1+z^2}\frac{\partial^2 z}{\partial\nabla\tilde{\rho}^2} - \frac{2*z}{(1+z^2)^2}\frac{\partial z}{\partial\nabla\tilde{\rho}}\left(\frac{\partial z}{\partial\nabla\tilde{\rho}}\right)^T + \\ &e^z\frac{\partial z}{\partial\nabla\tilde{\rho}}\left(\frac{\partial z}{\partial\nabla\tilde{\rho}}\right)^T + e^z\frac{\partial^2 z}{\partial\nabla\tilde{\rho}^2}\Bigg]\end{aligned} \tag{7.35}$$

where

$$\frac{\partial z}{\partial\nabla\tilde{\rho}} = \alpha\left[\frac{\boldsymbol{v}}{||\boldsymbol{v}||\,||\nabla\tilde{\rho}||} - \frac{(\nabla\tilde{\rho})^T\boldsymbol{v}(\nabla\tilde{\rho})}{||\boldsymbol{v}||\,||\nabla\tilde{\rho}||^3}\right] \tag{7.36}$$

$$\frac{\partial^2 z}{\partial\nabla\tilde{\rho}^2} = -\alpha\left[\frac{\boldsymbol{v}(\nabla\tilde{\rho})^T}{||\boldsymbol{v}||\,||\nabla\tilde{\rho}||^3} + \frac{(\nabla\tilde{\rho})\boldsymbol{v}^T}{||\boldsymbol{v}||\,||\nabla\tilde{\rho}||^3} + \frac{(\nabla\tilde{\rho})^T\boldsymbol{v}\boldsymbol{I}}{||\boldsymbol{v}||\,||\nabla\tilde{\rho}||^3} - 3\frac{(\nabla\tilde{\rho})^T\boldsymbol{v}(\nabla\tilde{\rho})(\nabla\tilde{\rho})^T}{||\boldsymbol{v}||\,||\nabla\tilde{\rho}||^5}\right] \tag{7.37}$$

By choosing the function $w(\nabla\tilde{\rho})$ as in equation (7.33) it acts as a step-function similar to the thresholding functions. Increasing the parameter β will provide a steeper slope thus affect the function more. The parameter c acts as the thresholding parameter and could be chosen to the value of the critical angle. From Figure 7.2 it is clear that in order to not violate the overhang constraint $\theta_0 \leq \theta$ which leads to $\cos(\theta) \leq \cos(\theta_0)$ which is illustrated in Figure 7.3a. In Figure 7.3b the function $w(\nabla\tilde{\rho})$ is plotted according to equation (7.33) with the parameters: $\boldsymbol{v}^T = [0, 1]$, $c = -\cos(45)$ and, $\beta = 10$ for the lower curve and $\boldsymbol{v}^T = [0, 1]$, $c = -\cos(45)$ and, $\beta = 11$ for the higher curve.

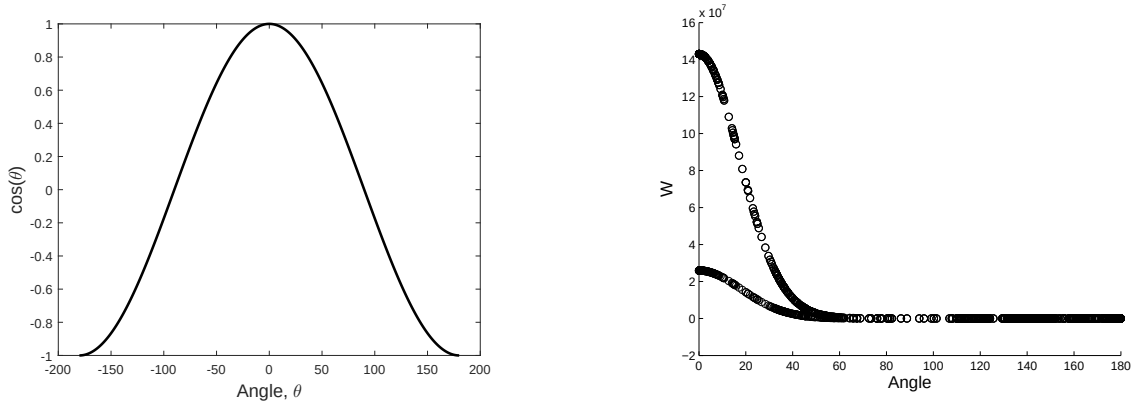

(a) $\cos(\theta)$ (b) The function $w(\nabla\tilde{\rho})$

Figure 7.3: Filter equation $w(\nabla\tilde{\rho})$.

7.3 Result and performance

The topology optimization is performed on a two dimensional MBB beam, where geometry and boundary conditions are depicted in Figure 7.4. The compliance is to be minimized with a volume constraint. The element discretization is performed with four-node rectangular elements.

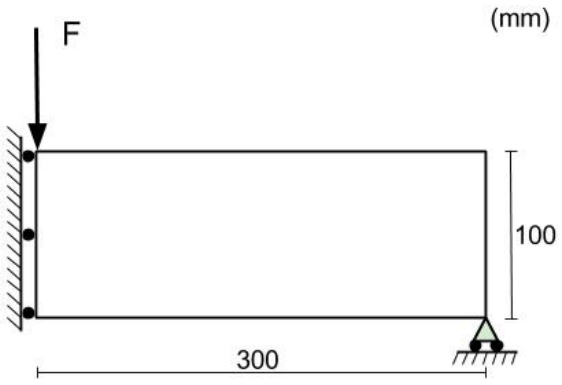

Figure 7.4: Illustration of the geometry and boundary conditions.

Figure 7.5a and Figure 7.5b show the result from the topology optimization solved using the MMA described in Section 3.2 for two different meshes, 14x42 and 40x120 elements. It has been solved using the SIMP approach described in Section 3.3 with the algorithmic parameter $p = 3$ and with modulus of elasticity $E = 1$. It can be observed that the numerical problems mentioned in Section 3.4 do appear in the solution. There are checkerboard regions where the solid and void alternates, mainly observed with the finer mesh in Figure 7.5b. Figure 7.5c and Figure 7.5d depicts the filtered design using Helmholtz density based PDE filter. The filter removes checkerboard pattern and introduces a length scale. The filtered designs will act as reference designs.

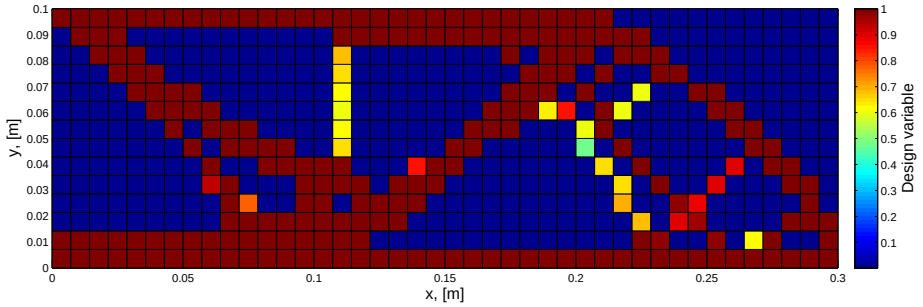

(a) No filter

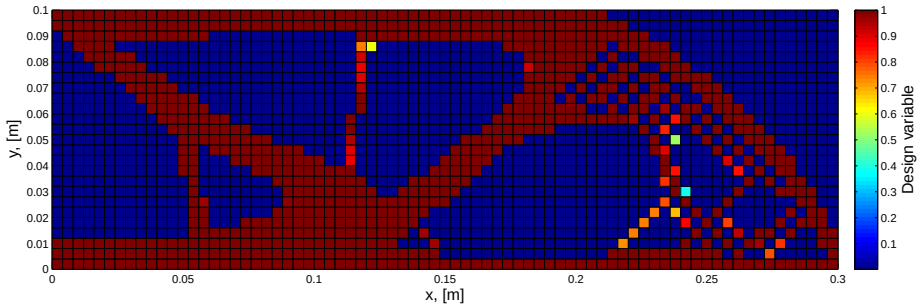

(b) No filter.

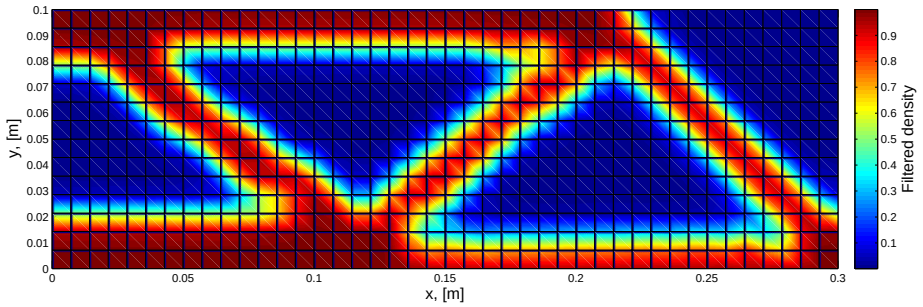

(c) Helmholtz density based PDE filter with the filter radius, $R = 0.55 *$ (element side lenght).

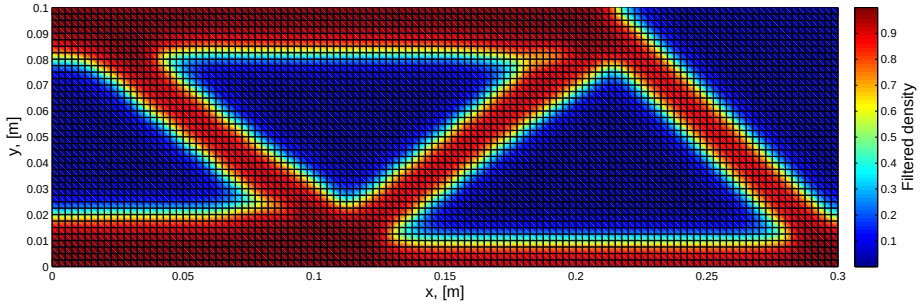

(d) Helmholtz density based PDE filter with the filter radius, $R = 1.5 *$ (element side lenght).

Figure 7.5: Optimized design for two different meshes.

The density gradient filter is tested on the two different meshes above in Figure 7.5 using the S-direction as baseplate with a vertical printing direction. The critical angle is as for the previous example set to 45°. Regions violating the overhang additive manufacturing constraint is mainly observed in the top regions but also in the tilted side bars. The

designs using different parameter values in the filter can be observed in Figure 7.6 for the coarse mesh and in Figure 7.7 for the fine mesh.

Starting with the coarse mesh, comparing Figure 7.6a , Figure 7.6b and, Figure 7.6c it can be observed that increasing the value of the β-parameter increases the affect of the filter as more bars, mainly leading from the upper regions is inserted. In the far left region the top region violating the overhang constraint is removed, however, a few of the inserted bars is on the verge of violating the angle of 45°. Increasing only the value of the r-parameter affect the design but not to the same extent as increasing the β-parameter, which is a reasonable result since the β-parameter increases the $w(\nabla\tilde{\rho})$-function exponentially. Continuing with the fine mesh in Figure 7.7 similar result is obtained, i.e. increasing the value of the β-parameter increases the affect of the filter as more bars, mainly leading from the upper regions is inserted. Increasing the value of the r-parameter affect the design but not to the same extent as increasing the β-parameter, mainly seen as the upper regions are not affected as much. In the fine mesh it is more clear that a few of the inserted bars either is on the verge of violating or violates the angle of 45°, mainly observed in Figure 7.7c. In all cases for both of the meshes it can be observed that the filtered densities obtain values greater than 1 and negative values in certain spots. In case 3 and case 4 in the fine mesh this was very extensive and was therefore scaled in order to obtain a more distinct structure. Neither of the cases in the fine or coarse mesh provides completely self supporting designs regarding the overhang constraint.

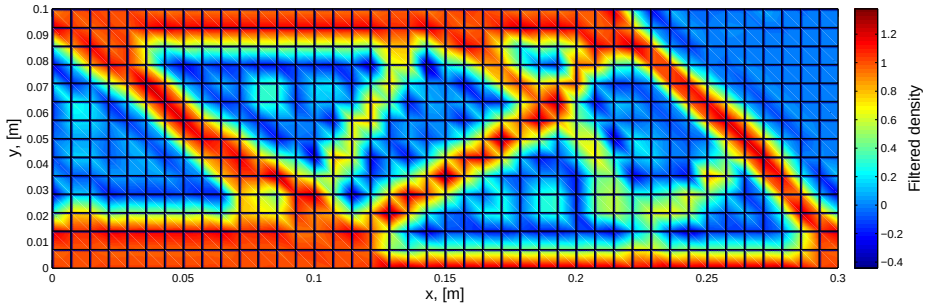

(a) Case 1 coarse mesh.
Parameters: $\beta = 40$, $r = 0.1*$(element side) and $c = -\cos(45)$. $\frac{C}{C_{ref}} = 0.861$

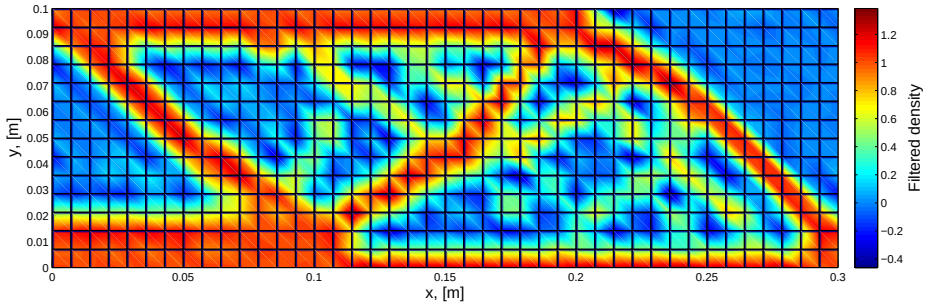

(b) Case 2 coarse mesh.
Parameters: $\beta = 50$, $r = 0.1*$(element side) and $c = -\cos(45)$. $\frac{C}{C_{ref}} = 0.927$

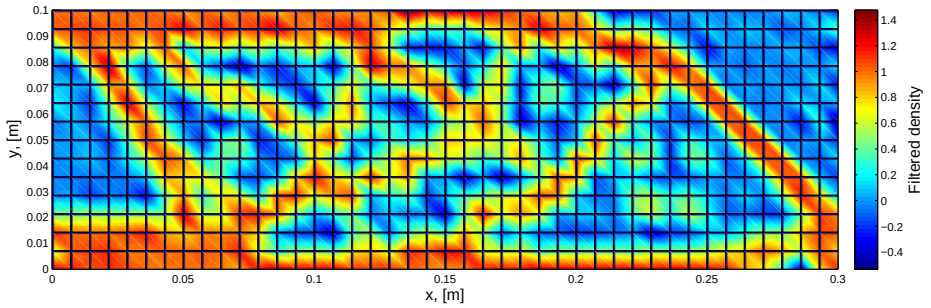

(c) Case 3 coarse mesh.
Parameters: $\beta = 60$, $r = 0.1*$(element side) and $c = -\cos(45)$. $\frac{C}{C_{ref}} = 0.893$

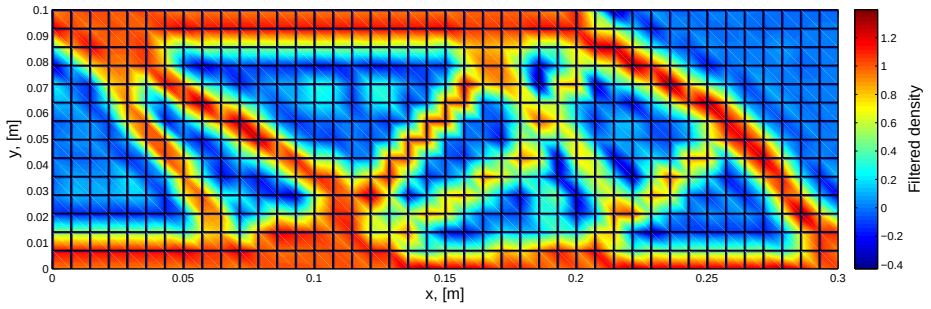

(d) Case 4 coarse mesh.
Parameters: $\beta = 20$, $r = 0.6*$(element side) and $c = -\cos(45)$. $\frac{C}{C_{ref}} = 0.902$

Figure 7.6: Density gradient filter coarse mesh.

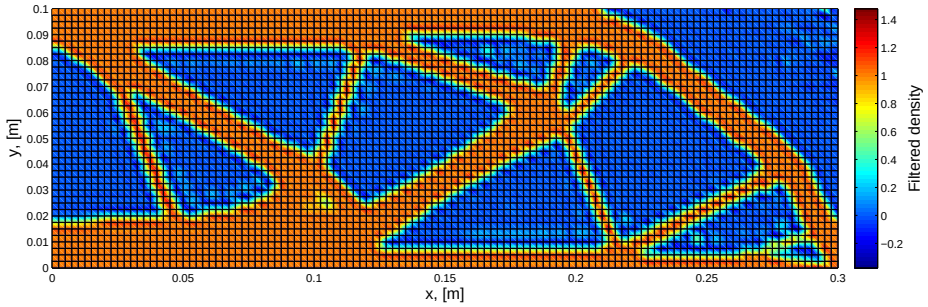

(a) Case 1 fine mesh.
Parameters: $\beta = 30$, $r = 0.1*$(element side) and $c = -\cos(45)$. $\frac{C}{C_{ref}} = 0.945$

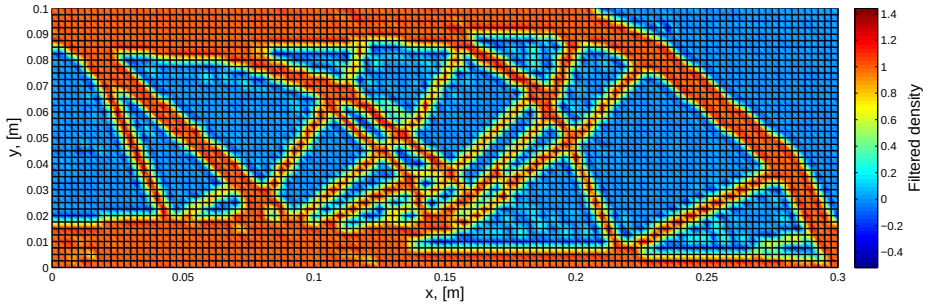

(b) Case 2 fine mesh.
Parameters: $\beta = 45$, $r = 0.1*$(element side) and $c = -\cos(45)$. $\frac{C}{C_{ref}} = 0.962$

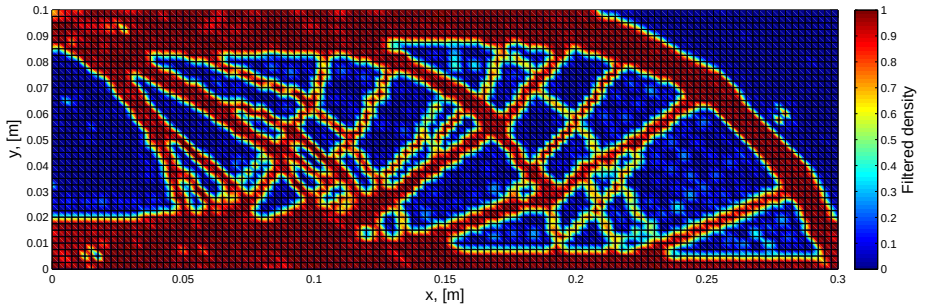

(c) Case 3 fine mesh.
Parameters: $\beta = 60$, $r = 0.1*$(element side) and $c = -\cos(45)$. $\frac{C}{C_{ref}} = 0.947$

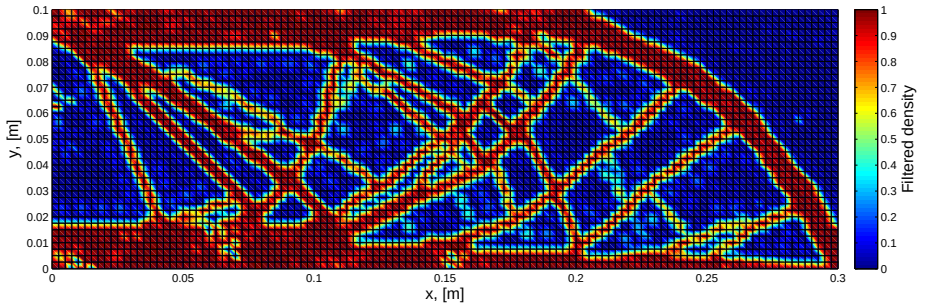

(d) Case 4 fine mesh.
Parameters $\beta = 40$, $r = 0.5*$(element side) and $c = -\cos(45)$. $\frac{C}{C_{ref}} = 1.078$

Figure 7.7: Density gradient filter fine mesh.

Chapter 8

Discussion and Further Work

The method proposed by Langelaar (2017) provides a self supporting design regarding the considered overhang constraint and is computationally efficient. However, the application becomes limited by the fact that the overhang angle is tied to the element discretization, and that the printing directions need to be axiparallel to the coordinate axis. The method is based on the neighbouring elements which result in that these either have to be registered and saved or be found in each iteration. Both become expensive operations for fine meshes or complex domains. In order to address these limitations a new method is proposed using Helmholtz density based PDE filter. Using the nodal values the density gradient of each element can be calculated and used to prevent undesirable designs.

The method uses the density gradient to alter the filter which affect the design and provides a different solution to the optimization problem. Certain regions violating the overhang constraints are changed for the better but the obtained design is still not completely self supporting. As shown in the previous examples the filter is very sensitive to the parameters, especially r and β. In order to obtain a more self supporting structure the parameter β is increased which causes numerical difficulties when solving the filter equation, leading to spots where the filtered density is much higher than 1 or even negative in some regions. However, if not increasing the parameter a self supporting design is not obtained. A thresholding filter, for instance the volume preserving Heaviside projection filter described in Section 3.5, would likely fix this problem and provide densities 0/1. Comparing the meshes would be hard as the parameters used are not optimized for each mesh respectively, but it can be concluded that the designs are affected similarly in both cases regarding the change of the parameters β and r. Similar to the previously discussed method proposed by Langelaar (2017) there are bars going into the side of other bars. This would as mentioned before cause a bending moment which would usually not be preferred in an optimal structure.

It would be more convenient to only use one parameter, i.e. reducing the formulation to only use the β-parameter to affect the design. However, the r-parameter is necessary to scale down the filter function in order for the residual function to be solved. Using only the β-parameter does not provide a self supporting design with the function $w(\boldsymbol{\nabla}\tilde{\rho})$ used in the proposed method. Other filter functions $w(\boldsymbol{\nabla}\tilde{\rho})$ should be further implemented and

tested. Adding the original filter, Helmholtz density based PDE filter, to the optimization in order to introduce a length scale in the entire design should also be considered. In the current method this is not included.

Another approach that should be further investigated is adding a constraint to the optimization problem targeting the overhang constraint. Using the same figure and constraint as before, where $\theta_0 \leq \theta$ and $\cos(\theta) \leq \cos(\theta_0)$ in order for the overhang constraint not to be violated, a constraint function can be formed where $\cos(\theta) - \cos(\theta_0) \leq 0$.

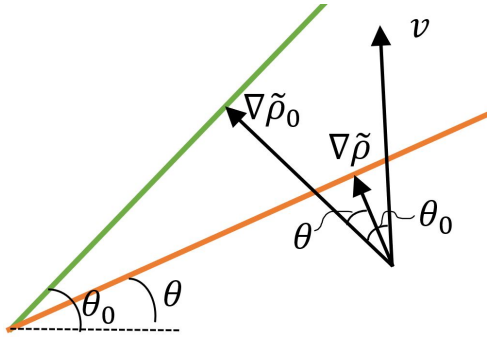

Figure 8.1: Illustration of the density gradient constraint.

In order to get a global constraint a p-norm functional defined in the entire domain could be used and the structural optimization problem becomes

$$\$\mathbb{O} = \begin{cases} \min\limits_{\boldsymbol{\rho}} & C = \boldsymbol{F}^T\boldsymbol{u}(\boldsymbol{\rho}) \\ s.t. & \begin{cases} \sum_{i=1}^{N} v_i\rho_i - V_{max} \leq 0 \\ \left[\sum_{i=1}^{N}\left(\frac{n\nabla\tilde{\rho}_i}{\|n\|\|\nabla\tilde{\rho}_i\|} - \cos(\theta_0)\right)^P\right]^{\frac{1}{P}} \leq 0 \\ \rho_{min} \leq \rho_i \leq \rho_{max}, \quad i = 1,..,N \end{cases} \end{cases}$$

This approach should be further addressed in future work, to be implemented and tested.

Bibliography

Andreassen, E., Clausen, A., Schevenels, M., Lazarov, B. S., and Sigmund, O. (2011). Efficient topology optimization in matlab using 88 lines of code. *Structural and Multidisciplinary Optimization*, 43(1):1–16.

ANSYS (12/10-2017). Ansys mechanical. http://www.ansys.com/products/structures/topology-optimization.

Bendsøe, M. P. and Kikuchi, N. (1988). Generating optimal topologies in structural design using a homogenization method. *Computer Methods in Applied Mechanics and Engineering*, 71(2):197 – 224.

Bendsøe, M. P. and Sigmund, O. (2004). *Topology optimization : theory, methods and applications.* Berlin : Springer, c2004.

Bendsøe, M. P. (1989). Optimal shape design as a material distribution problem. *Structural optimization*, 1(4):193–202.

Bourdin, B. (2001). Filters in topology optimization. *International Journal for Numerical Methods in Engineering*, 50(9):2143–2158.

Brackett, D., Ashcroft, I., and Hague, R. (2011). Topology optimization for additive manufacturing. In *Proceedings of the solid freeform fabrication symposium, Austin, TX*, volume 1, pages 348–362. S.

Bruns, T. E. and Tortorelli, D. A. (2001). Topology optimization of non-linear elastic structures and compliant mechanisms. *Computer Methods in Applied Mechanics and Engineering*, 190(26):3443 – 3459.

Christensen, P. W., Gladwell, G. M. L., and Klarbring, A. (2008). *An introduction to structural optimization.* Solid Mechanics and Its Applications: 153. Dordrecht : Springer Netherlands, 2008.

Clausen, A. (2016). *Topology Optimization for Additive Manufacturing.* PhD thesis, Technical University of Denmark.

Fleury, C. and Braibant, V. (1986). Structural optimization: a new dual method using mixed variables. *International journal for numerical methods in engineering*, 23(3):409–428.

Gardan, J. (2016). Additive manufacturing technologies: state of the art and trends. *International Journal of Production Research*, 54(10):3118–3132.

Gaynor, A. T. and Guest, J. K. (2016). Topology optimization considering overhang constraints: eliminating sacrificial support material in additive manufacturing through design. *Structural and Multidisciplinary Optimization*, 54(5):1157.

Gibson, I., Rosen, D., and Stucker, B. (2015). *Additive Manufacturing Technologies. [Elektronisk resurs] : 3D Printing, Rapid Prototyping, and Direct Digital Manufacturing.* New York, NY : Springer New York : Imprint: Springer, 2015.

Guest, J. K., Prévost, J. H., and Belytschko, T. (2004). Achieving minimum length scale in topology optimization using nodal design variables and projection functions. *International Journal for Numerical Methods in Engineering*, 61(2):238–254.

Langelaar, M. (2016). Topology optimization of 3d self-supporting structures for additive manufacturing. *Additive Manufacturing*, 12:60 – 70.

Langelaar, M. (2017). An additive manufacturing filter for topology optimization of print-ready designs. *Structural and Multidisciplinary Optimization*, 55(3):871–883.

Lazarov, B. S. and Sigmund, O. (2011). Filters in topology optimization based on helmholtz-type differential equations. *International Journal for Numerical Methods in Engineering*, 86(6):765–781.

Leary, M., Merli, L., Torti, F., Mazur, M., and Brandt, M. (2014). Optimal topology for additive manufacture: A method for enabling additive manufacture of support-free optimal structures. *Materials and Design*, 63(1):678.

Li, C., Liu, J., and Guo, Y. (2016). Prediction of residual stress and part distortion in selective laser melting. *Procedia CIRP*, 45:171 – 174. 3rd CIRP Conference on Surface Integrity.

OptiStruct, A. (04/07-2017). Optistruct overview. http://www.altairhyperworks.com/Product/OptiStruct.

Poulsen, T. A. (2003). A new scheme for imposing a minimum length scale in topology optimization. *International Journal for Numerical Methods in Engineering*, 57(6):741–760.

Quhao, L., Wenjiong, C., Shutian, L., and Liyong, T. (2016). Structural topology optimization considering connectivity constraint. *Structural and Multidisciplinary Optimization*, 54(4):971 – 984.

Saabye Ottosen, N. and Ristinmaa, M. (2005). *The mechanics of constitutive modeling. [Elektronisk resurs].* Amsterdam : Elsevier, cop. 2005.

Shutian, L., Quhao, L., Wenjiong, C., Liyong, T., and Gengdong, C. (2015). An identification method for enclosed voids restriction in manufacturability design for additive manufacturing structures. *Frontiers of Mechanical Engineering*, 10(2):126 – 137.

Sigmund, O. (1997). On the design of compliant mechanisms using topology optimization. *Mechanics of Structures and Machines*, 25(4):493–524.

Sigmund, O. (2007). Morphology-based black and white filters for topology optimization. *Structural and Multidisciplinary Optimization*, 33(4):401–424.

Sigmund, O. and Petersson, J. (1998). Numerical instabilities in topology optimization: A survey on procedures dealing with checkerboards, mesh-dependencies and local minima. *Structural optimization*, 16(1):68–75.

Svanberg, K. (1987). The method of moving asymptotes—a new method for structural optimization. *International Journal for Numerical Methods in Engineering*, 24(2):359–373.

Thomas, D. (2010). *The development of design rules for selective laser melting*. PhD thesis, University of Wales Institute, Cardiff.

Thompson, M. K., Moroni, G., Vaneker, T., Fadel, G., Campbell, R. I., Gibson, I., Bernard, A., Schulz, J., Graf, P., Ahuja, B., and Martina, F. (2016). Design for additive manufacturing: Trends, opportunities, considerations, and constraints. *CIRP Annals - Manufacturing Technology*, 65(2):737 – 760.

Vanek, J., Galicia, J., and Benes, B. (2014). Clever support: Efficient support structure generation for digital fabrication. *Computer Graphics Forum*, 33(5):117 – 125.

Wang, D., Yang, Y., Yi, Z., and Su, X. (2013). Research on the fabricating quality optimization of the overhanging surface in slm process. *The International Journal of Advanced Manufacturing Technology*, 65(9):1471–1484.

Xu, S., Cai, Y., and Cheng, G. (2010). Volume preserving nonlinear density filter based on heaviside functions. *Structural and Multidisciplinary Optimization*, 41(4):495–505.

Zhou, M., Lazarov, B., Wang, F., and Sigmund, O. (2015). Minimum length scale in topology optimization by geometric constraints. *Computer Methods in Applied Mechanics and Engineering*, 293:266–282.

Zhou, M. and Rozvany, G. (1991). The coc algorithm, part ii: Topological, geometrical and generalized shape optimization. *Computer Methods in Applied Mechanics and Engineering*, 89(1):309 – 336. Second World Congress on Computational Mechanics.